AD 400 730

63-37

Department of AERONAUTICS and ASTRONAUTICS
STANFORD UNIVERSITY

J. FERNANDEZ-SINTES
W. H. HORTON
N. J. HOFF

THERMAL BUCKLING OF ANNULAR PLATES

DECEMBER
1962

PREPARED FOR THE AIR FORCE OFFICE OF SCIENTIFIC RESEARCH
UNDER GRANT NO. AF-AFOSR-62-146

SUDAER
NO. 143

Department of Aeronautics and Astronautics
Stanford University
Stanford, California

THERMAL BUCKLING OF ANNULAR PLATES

by

Julio J. Fernandez-Sintes, Wilfred H. Horton
and Nicholas J. Hoff

SUDAER No.143
December 1962

The work here reported was performed under
research grant No. AF-AFOSR-62-146

ACKNOWLEDGMENT

The authors are grateful to Lt. Col. W. B. Higgins, USMC and Lt. D. W. Mathews, USN, who initiated the development of the methods and the equipment (as part of their Engineer's theses) upon which the improved versions here described are based.

TABLE OF CONTENTS

LIST OF ILLUSTRATIONS

LIST OF ILLUSTRATIONS (Cont'd)

NOTATION

a	inner radius of annular plate
b	outer radius of annular plate
D	flexural rigidity of the plate
E	modulus of elasticity
F_o	radial heat flux at $r = a$
h	thickness of plate
K	thermal conductivity
r	radius
T	increment of temperature
T_o	increment of temperature at $r = a$
t	time
u	radial displacement
w	lateral displacement of an element of the plate
w_i	initial lateral deflection of the plate
w_o	additional lateral deflection of the inner edge of the annular plate
w_{io}	initial lateral deflection of the inner edge of the annular plate
α	coefficient of thermal expansion
θ	$= T/T_o$; nondimensional increment of temperature
κ	thermal diffusivity
ν	Poisson's ratio
ρ	$= r/b$; nondimensional radius
σ_r	radial stress
τ_o	parameter defined by Eq.(2.2.11)

NOTATION (Cont'd)

φ	= dw/dr ; radial slope of a deflected element of the plate
φ_i	initial radial slope of the plate
ψ	function of ρ defined by Eq.(2.2.10)

INTRODUCTION

Heat energy may cause the failure of a structure in a number of ways; in particular, thermal stresses may cause instability of the configuration of a structural element.

This report summarizes the methods and conclusions of an investigation on thermally induced instability of annular plates. The research work here described is limited to cases in which the temperature variation is symmetric about the axis of the annular plate. Moreover, the temperature is assumed to be uniform across the thickness of the plate. Additional simplifying assumptions will be listed later.

In the first section of this report, consideration is given to the problem of determining the radial temperature distribution corresponding to prescribed boundary conditions.

In the second section the problem of determining theoretically the occurrence of instability for a given plate and a given transient temperature distribution is analyzed and a method is presented to obtain approximate solutions. The method is applied to two different cases: in the first the temperature distribution is obtained theoretically and corresponds to idealized heat transfer conditions; and in the second the temperature distribution is assumed to be known from an experimental investigation.

The effect of initial imperfections in the flatness of the plate is considered and a Southwell plot is used to determine the critical temperature from experimental data when the initial imperfections are small and axisymmetric.

The third section is a summary of the experimental methods applied to the collected data on temperature and deflections. A description of the tests performed is presented and the results are compared with the theoretical predictions.

Finally, an appendix covers the interpretation of the interference fringes that are obtained by the Moiré technique.

SECTION I

THE AXISYMMETRIC PROBLEM OF HEAT TRANSFER IN A CIRCULAR PLATE

1.1 General Problem

In the general case the plate under consideration may receive heat energy through conduction from an internal heat source or through convection or radiation from an external source. In either case it is assumed that the heat input through the boundary of the plate is axisymmetric. During the transient period the heat flows through the plate in accordance with the laws of conduction and is partially stored in the plate and partially dissipated to the environment by convection and radiation. When the steady state is reached the heat dissipation to the environment balances the heat input and the heat stored remains constant.

The general problem, as stated above, is nonlinear and difficult to solve. No attempt will be made here to solve it. Instead, simplifying assumptions will be introduced in order to linearize the problem.

1.2 Heat Transfer without Dissipation to the Environment

When the assumption is made that no heat transfer occurs from the lateral surfaces of the plate to the environment, the problem is linear and is analogous to that of an infinite cylinder.

Solutions to this problem for different boundary conditions are readily available (see Ref.1). A particular case of interest will be treated here.

1.2.1 Annular Plate with Constant Flux at the Inner Edge and Zero Temperature at the Outer Edge

The solution to the case of constant flux, F_o , at the inner edge ($r = a$), and zero temperature at the outer edge ($r = b$) is:

$$T = \frac{aF_o}{K} \ln \frac{b}{r} + \frac{\pi F_o}{K} \sum_{n=1}^{\infty} e^{-\kappa \alpha_n^2 t} \frac{J_o^2(b\alpha_n)\left[J_o(r\alpha_n)Y_1(a\alpha_n) - Y_o(r\alpha_n)J_1(a\alpha_n)\right]}{\alpha_n\left[J_1^2(a\alpha_n) - J_o^2(b\alpha_n)\right]} \qquad (1.2.1.1)$$

where the α_n are the positive roots of the equation

$$J_1(a\alpha)Y_o(b\alpha) - Y_1(a\alpha)J_o(b\alpha) = 0 \qquad (1.2.1.2)$$

In the experimental part of this research a number of tests were conducted for an annular plate specimen of the following characteristics:

Material:	mild steel	
Inner radius:	$a = 1.5$ in.	(1.2.1.3)
Outer radius:	$b = 5$ in.	
Diffusivity:	$\kappa = 0.12$ cm^2/sec	

With these particular values the first three roots of equation (1.2.1.2) are:

$$\alpha_1 = 0.2194 \text{ cm}^{-1}$$
$$\alpha_2 = 0.5507 \text{ cm}^{-1} \qquad (1.2.1.4)$$
$$\alpha_3 = 0.8966 \text{ cm}^{-1}$$

After substitution of these values in (1.2.1.1) the expression $(T/F_o)K$ can be plotted versus r for particular values of the total heating time t. In Fig.1 this has been done for $t = 50$, 100, 200, 400 sec and for $t = \infty$ (steady state).

For values of time lower than 50 seconds, more than three roots α_n would be required in the calculations. If $\theta = T/T_o$ and $\rho = r/b$ are introduced, where T_o is the temperature at the inner edge ($r = a$) a nondimensional plot of the temperature distribution for the particular plate under consideration is obtained (Fig.2). It is interesting to note that θ is independent of the heat flux F_o.

1.3 Heat Transfer with Dissipation to the Environment. Experimental Survey

In the absence of a theoretical solution accounting for the dissipation of heat to the environment, an experiment was performed to estimate the order of magnitude of the effect on the temperature distribution. An annular plate of the dimensions specified in (1.2.1.3) was rigidly supported at its outer edge by means of a massive ring, so as to reproduce closely the boundary condition $T = 0$ at $r = b$ of 1.2.1. An electrical heater located in the center of the annular plate provided a heat source of reasonably constant heat flux at $r = a$.

Figure 3 is a plot of the temperature variation with time for a number of points on the plate. The irregular behavior noticeable between 0 and 30 seconds corresponds to the period which the heater requires to attain steady temperature.

Figure 4 is a plot of the temperature distribution in the plate for different values of time. This is again plotted nondimensionally in Fig.5.

The temperature distributions for $t = 200$ from Figs. 2 and 5 are superimposed in Fig.6 for the purpose of comparison. The comparison is particularly significant due to the fact that the nondimensional temperature distribution in the idealized case is independent of the heat flux.

SECTION II

LINEARIZED THEORY OF THE AXISYMMETRICAL THERMAL BUCKLING OF ANNULAR PLATES

2.1 Basic Assumptions

Small deflections are assumed, as is the case at the onset of buckling, and consequently the usual assumptions of the theory of thin plates with small deflections will be made.

Temperature distribution and edge conditions are perfectly axisymmetric. The annular plate is perfectly flat, of uniform thickness at a uniform temperature and free from stresses in its initial state. Temperature variations through the thickness are neglected. The material is perfectly elastic, homogeneous and isotropic.

2.2 Differential Equation for Axisymmetrical Bending

The equation of equilibrium in the lateral direction of an element of the plate in cylindrical coordinates can be written (Ref.2)

$$\frac{d}{dr}\left[\frac{1}{r}\frac{d}{dr}(r\varphi)\right] = -\frac{Q}{D} \tag{2.2.1}$$

where Q denotes the shearing force per unit length of the cylindrical section of radius r.

With the assumption of small deflections and in the absence of lateral loads, the shearing force satisfies the following relation:

$$Q = (\sigma_r h)\varphi \tag{2.2.2}$$

Substitution in (2.2.1) yields

$$\frac{d}{dr}\left[\frac{1}{r}\frac{d}{dr}(r\varphi)\right] + \frac{\sigma_r h}{D}\varphi = 0 \tag{2.2.3}$$

which is a linear homogeneous second-order equation in φ. σ_r is given by the equation (Ref.3)

$$\sigma_r = -\alpha E \frac{1}{r^2}\int_a^r Trdr + \frac{E}{1-\nu^2}\left[c_1(1+\nu) - c_2(1-\nu)\frac{1}{r^2}\right] \qquad (2.2.4)$$

where c_1, c_2 are determined by the boundary conditions. In the case of an annular plate with fixed outer boundary and free inner boundary the boundary conditions are:

$$\begin{aligned} (\sigma_r)_{r=a} &= 0 \\ (u)_{r=b} &= 0 \end{aligned} \qquad (2.2.5)$$

where u is the radial displacement given by

$$u = (1+\nu)\,\alpha\,\frac{1}{r}\int_a^r Trdr + c_1 r + c_2\frac{1}{r} \qquad (2.2.6)$$

Substitution yields:

$$\sigma_r = -\frac{\alpha E}{r^2}\left[\frac{(r^2-a^2)(1+\nu)}{b^2(1-\nu)+a^2(1+\nu)}\int_a^b Trdr + \int_a^r Trdr\right] \qquad (2.2.7)$$

If the nondimensional parameters

$$\begin{aligned} \rho &= r/b \qquad (a/b \le \rho \le 1) \\ \theta(\rho) &= T(\rho)/T_o \end{aligned} \qquad (2.2.8)$$

are introduced, where T_o is the temperature at $r = a$, and are substituted in equations (2.2.7) and (2.2.3), the differential equation (2.2.3) can be written in the form

$$\frac{d}{d\rho}\left[\frac{1}{\rho}\frac{d}{d\rho}(\rho\varphi)\right] = -\tau_o\psi\varphi \qquad (2.2.9)$$

where

$$\psi = \frac{1}{\rho^2}\left[\frac{(\rho^2 b^2 - a^2)(1+\nu)}{b^2(1-\nu) + a^2(1+\nu)} \int_{a/b}^{1} \theta\rho d\rho + \int_{a/b}^{\rho} \theta\rho d\rho\right] \qquad (2.2.10)$$

and

$$\tau_o = 12(1-\nu^2)\frac{b^2}{h^2}\alpha T_o \qquad (2.2.11)$$

with the boundary conditions

$$\begin{aligned} (\varphi)_{\rho=1} &= 0 \quad \text{(zero slope at } \rho = 1\text{)} \\ \left(\frac{d\varphi}{d\rho} + \nu\frac{\varphi}{\rho}\right)_{\rho=a/b} &= 0 \quad \text{(zero moment at } \rho = a/b\text{)} \end{aligned} \qquad (2.2.12)$$

and

$$(V)_{\rho=1} = \left| D\frac{d}{d\rho}\left\{\frac{1}{\rho}\frac{d}{d\rho}(\rho\varphi)\right\}\right|_{\rho=1} = 0 \quad \text{(shear force at } \rho = 1\text{)}$$

This last boundary condition is identical with equation (2.2.9) for $\rho = 1$, when the condition $(\varphi)_{\rho=1} = 0$ is applied. This is due to the fact that equation (2.2.9) is the equation of equilibrium in the lateral direction of an element of the plate. The condition of zero shear force at the inner edge is also satisfied by equation (2.2.9) as a consequence of condition (2.2.5), $(\sigma_r)_{r=a} = 0$. This condition, applied to (2.2.3) results in $(V)_{r=a} = 0$.

The determination of φ reduces to the boundary-value problem of solving equation (2.2.9) with the boundary conditions (2.2.12).

The term ψ (2.2.10) is a function of ρ determined by the geometrical and elastic characteristic of the plate and the temperature distribution in the plate.

2.3 Determination of the Critical Temperature

In the case of differential equation (2.2.9), $\varphi \equiv 0$ is always a solution of the problem. Solutions with $\varphi \neq 0$ can be found only for discrete values of the parameter τ_o. Physically this means that the plate may adopt different modes of deflection for corresponding different discrete values of the temperature T_o. The least of these values will be taken as the critical temperature T_{crit}. It can be shown from energy consideration that

if $T_o < T_{crit}$, $\varphi \equiv 0$ is the stable state of equilibrium

if $T_o > T_{crit}$, $\varphi \equiv 0$ is unstable and some solution $\varphi \neq 0$ is stable.

Exact solutions of equation (2.2.9) cannot be found readily for prescribed temperature distributions, but several approximate methods are available to solve the problem.

2.4 Application of the Stodola-Vianello Method to the Determination of the Critical Temperature

The Stodola-Vianello method (see Ref.4) is a method of successive approximations which gives a sequence of functions that converge precisely to the first characteristic value.

Two successive integrations of equation (2.2.9) yield the expression

$$\varphi = -\tau_o \left[\frac{1}{\rho} \int_{\rho_o}^{\rho} \rho \left(\int_{\rho_o}^{\rho} \psi\varphi d\rho \right) d\rho + c_1\rho + c_2 \frac{1}{\rho} \right] \qquad (2.4.1)$$

The method consists of starting with a conveniently chosen first approximation φ_1 to φ in the right side of (2.4.1). After the two successive integrations are completed, c_1 and c_2 are determined in such a manner that the expression within the brackets satisfies the boundary conditions. This will result in

$$\varphi_2 = \tau_o f_1(\rho) \qquad (2.4.2)$$

If the approximation φ_1 had been the characteristic function then $\varphi_2 \equiv \varphi_1$ and the corresponding characteristic value of τ would be given by

$$\tau_o = \frac{\varphi_1(\rho)}{f_1(\rho)} \tag{2.4.3}$$

The first approximation, $\varphi_1(\rho)$ will in general not give a constant ratio. If φ_2 is taken as the improved approximation and the cycle repeated, it can be shown that the ratio $\varphi_n(\rho)/f_n(\rho)$ tends to a constant value over the interval $(\rho_o,1)$ as n is increased; and that this constant value is the lowest characteristic value τ.

Successive estimates of the characteristic value may be obtained after each cycle by requiring that the functions ρ_n and $\varphi_{n+1} = \tau_o f_n$ agree as well as possible (in some sense) over the interval. One possible formulation is

$$\tau_n = \frac{\int_{\rho_o}^{1} \varphi_n(\rho)d\rho}{\int_{\rho_o}^{1} f_n(\rho)d\rho} \tag{2.4.4}$$

The method can be carried out either algebraically or graphically. However, difficulties are encountered in our particular case when an algebraical treatment is attempted. The temperature distribution θ is, in most cases, not easily expressible mathematically, and even when this is done, it usually results in complicated expressions for ψ which make the integrations cumbersome. It is preferable therefore to carry out the work graphically (see Fig.9).

From a plot of the nondimensional temperature distribution θ versus the nondimensional radius ρ, function ψ is computed numerically. Next, the first approximation φ_1 to the slope function is selected. The rapidity of the convergence of the method depends on this selection.

The simplest algebraic expression that satisfies the boundary conditions (2.2.12) is

$$\varphi_1 = \rho^2 + \left[\frac{\nu/\rho_o - \rho_o(2+\nu)}{(1+\nu) - \nu/\rho_o}\right](\rho-1) - 1 \qquad (2.4.5)$$

This function gives a very fast convergence since it is a good approximation to the actual slope function (see Section III, Fig.33).

Next the product $\psi\varphi_1$ is computed numerically and plotted. The first integration is performed and the product

$$\rho I_1 = \rho \int_{\rho_o}^{\rho} \psi\varphi_1 d\rho \qquad (2.4.6)$$

is plotted. In the following step the second integration is carried out, the result divided by ρ, and the boundary conditions are applied to determine c_1 and c_2. This yields

$$f_1(\rho) = \frac{1}{\rho}\int_{\rho_o}^{\rho} \rho\left(\int_{\rho_o}^{\rho} \psi\varphi_1 d\rho\right)d\rho + c_1\rho + c_2\frac{1}{\rho} \qquad (2.4.7)$$

Next $f_1(\rho)$ is plotted and the first approximation to the characteristic value τ_o is obtained from

$$\tau_{o_1} = \frac{\int_{\rho_o}^{1} \varphi_1 d\rho}{\int_{\rho_o}^{1} f_1 d\rho} \qquad (2.4.8)$$

and the characteristic function from

$$\varphi_2 = \tau_{o_1} f_1 \qquad (2.4.9)$$

Because the first approximation is good, due to the already mentioned suitability of the approximation given in (2.4.5) to the problem under consideration, one cycle of the calculations suffices to determine an acceptable value of τ_o .

The critical temperature is then given by (2.2.11):

$$(\tau_o)_{crit} = \tau_o \frac{h^2}{12(1-\nu^2)b^2\alpha} \qquad (2.4.10)$$

It is of interest to remark that τ_o is determined only by the parameters a, b and the Poisson ratio, plus the temperature distribution and the boundary conditions, that is

$$\tau_o = \tau_o\left(a,b,\nu,\theta(\rho) \text{ , boundary conditions}\right)$$

but is independent of the thickness of the plate. Equation (2.4.10) can be written, if so desired, as

$$\left(\frac{T_o}{h^2}\right)_{crit} = \tau_o \frac{1}{12(1-\nu^2)b^2\alpha} \qquad (2.4.11)$$

2.4.1 Remarks on the Applicability of the Method

In the preceding paragraph a method was discussed that, starting from a particular nondimensional temperature distribution $\theta(\rho)$, yields the corresponding value of the critical edge temperature.

Most practical problems of heating result in transient conditions in which θ is a function of time $\theta = \theta(\rho,t)$. If this is the case, successive approximations are necessary to determine the critical temperature. The method given in 2.4 can be applied to determine critical temperature values for a number of values of t , so that a plot of T_{cr} versus time can be obtained. If the edge temperature $T_o(t)$ versus time is plotted on the same graph the intersection of the two curves yields both T_{cr} and t_{cr} .

2.5 Application to a Particular Idealized Case: Thermal Buckling of an Annular Plate with Constant Heat Flux at the Inner Free Edge, Zero Temperature at the Fixed Outer Edge and no Dissipation of Heat to the Environment

In paragraph 1.2.1 the temperature distribution corresponding to a particular annular plate, characterized by the parametric values given in (1.2.1.3), was obtained and the results plotted in Figs.1 and 2. It was found that the temperature is proportional to the heat flux. The following relation can be written

$$T(\rho) = f(\rho,t)F_o \qquad (2.5.1)$$

and in particular, for the temperature at the inner edge

$$T_o = f(t)F_o \qquad \text{(Fig.8)} \qquad (2.5.2)$$

On the other hand, $\theta = T/T_o$ (Fig.2) is independent of F_o. If we assume that buckling occurs at a particular time, for instance $t = 50$ sec, we can calculate from Fig.2, which provides θ_{50}, the corresponding critical temperature $(T_o)_{crit_{50}}$.

From Fig.8 we know that for $t = 50$ sec

$$(1000\ T/T_o)_{t=50} = 2.686$$

If $T_o = (T_o)_{crit_{50}}$ we obtain the value of F_o for which $t_{cr} = 50$ sec:

$$F_o = \frac{1000}{2.686}\,(T_o)_{crit_{50}}$$

This procedure has been used when

$$t = 50,\ 100,\ 200,\ 400 \text{ sec, and } t = \infty$$

and the results have been plotted in Fig.9.

The thickness of the plate has been left as a design parameter in accordance with (2.4.11).

Some interesting conclusions can be drawn from Fig.9.

(a) There is a particular value of F_o/h^2, that we shall call $(F_o/h^2)_{crit}$, such that

for $F_o/h^2 \leq (F_o/h^2)_{crit}$ buckling does not occur;

and

for $F_o/h^2 > (F_o/h^2)_{crit}$ buckling occurs after a finite time $t = t_{cr}$.

The critical value $(F_o/h^2)_{crit}$ is obtained by assuming that buckling occurs at $t = \infty$ and by taking the nondimensional temperature distribution in the steady state as the nondimensional temperature distribution at buckling.

The corresponding value of $(T_o/h^2)_{crit}$ is a minimum and can be taken as a lower bound on the heat flux.

(b) For $F_o/h^2 > (F_o/h^2)_{crit}$ the larger F_o/h^2, the larger $(T_o/h^2)_{crit}$ and the smaller t_{cr}. When F_o/h^2 tends to ∞, $t_{cr} \to 0$ and $(T_o/h^2)_{crit}$ tends to ∞.

This can be proved by considering the process of graphical calculation which leads to the determination of $(T_o/h^2)_{crit}$. If it is assumed that buckling occurs after an infinitesimal period of time, the corresponding nondimensional temperature distribution θ will be a line very close to the axis of abscissas and the area under this line will be infinitesimal.

The successive integrations lead to an expression of the following type:

$$\varphi = -\tau_o \left[\epsilon(\rho) + c_1\rho + c_2 \frac{1}{\rho}\right] = -\tau_o f_1(\rho)$$

where $\epsilon(\rho)$ is an infinitesimal. If the boundary conditions

$$\left.\begin{array}{ll} f_1(1) = 0 & c_1 + c_2 = \epsilon \\ \dfrac{\partial f_1}{\partial \rho} + \nu \dfrac{f_1}{\rho} = 0 & c_2 = Ac_1 \end{array}\right\} \qquad \begin{array}{l} c_1 = \dfrac{\epsilon}{1+A} \\ c_2 = \dfrac{A}{1+A}\,\epsilon \end{array}$$

are applied, one obtains

$$f_1(\rho) = \epsilon$$

and

$$\tau_o = \frac{\int \varphi_1 d\rho}{\int f_1 d\rho} = \frac{\text{finite}}{\int \epsilon d\rho} \to \infty$$

Hence

$$\left(\frac{T_o}{h^2}\right)_{crit} \to \infty$$

Now, from Fig.8 we see that

$$\lim_{t \to 0} \frac{T_o}{F_o} = 0$$

Consequently

$$\lim_{t \to 0} F_o \to \infty$$

Figures 8 and 9 are combined in Fig.10, where $(T_o/h^2)_{crit}$ and T_o/h^2, are plotted against time for different values of F_o/h^2. For any given value of F_o/h^2, the intersection of the corresponding curve T_o/h^2 with the curve $(T_o/h^2)_{crit}$ determines the critical time and the critical temperature. The conclusions drawn under (a) and (b) are visible from Fig.10. For values of F_o/h^2 smaller than $(F_o/h^2)_{crit}$ there is no intersection, which means that buckling does not occur.

2.6 Application to Experiment: Thermal Buckling of an Annular Plate Centrally Heated at the Inner Free Edge and Fixed at the Outer Edge

In paragraph 1.3 a summary was given of an experimental study of the temperature distribution over a particular specimen plate under specified heating and boundary conditions. The details of the experiment are described in Section III.

Figures 3, 4 and 5 summarize the experimental data obtained regarding the temperature distribution during periods of time ranging from 0 to 300 seconds; zero corresponds to the time when the heat is applied. The time of buckling can be determined in a first approximation by applying the method described in 2.4 and 2.4.1.

Starting from the values of θ plotted in Fig.5, the corresponding values of $(T_o/h^2)_{crit}$ are calculated and plotted against time (Fig.11). Next the values of T_o/h^2 measured during the process of heating are plotted against time on the same graph. The intersection of $(T_o/h^2)_{crit}$ and T_o/h^2 determines the critical point

In this particular case the critical values are

$$t_{cr} = 148 \text{ sec}$$

$$\left(\frac{T_o}{h^2}\right)_{crit} = 35{,}500 \ \frac{^oF}{in.^2}$$

The thickness of the plate used in the experiment was

$$h = 0.058 \text{ in.}$$

With this value one obtains

$$(T_o)_{crit} = 119.5^oF$$

For the purpose of comparison the curve $(T_o/h^2)_{crit}$ corresponding to the idealized case in which dissipation to the environment was neglected, is plotted as a dashed line in the same graph.

In article 2.6 it was noted that the curve $(T_o/h^2)_{crit}$ in the idealized case was an invariant with respect to the heat flux at the heat source. Whether this applies to practical cases with dissipation to the environment, is a problem that requires further investigation. Such an investigation could consist of an attempt to determine theoretically the temperature distribution when dissipation to the environment is taken into consideration, or an extensive series of tests from which data on the temperature distribution for different values of the heat flux could be obtained.

In article 2.6 it was found that a critical value of the heat flux F_o and a lower bound for $(T_o/h^2)_{crit}$ could be determined from consideration of the steady-state temperature distribution. If the steady-state temperature distribution for the case considered in this article were known, an asymptote could be determined for the curve $(T_o/h^2)_{crit}$ and the corresponding critical value of F_o and lower bound of $(T_o/h^2)_{crit}$ could be found.

2.7 Effect of Initial Imperfections

Let us assume that the initial deflection of the plate is axisymmetric, is small compared with the thickness of the plate, and is denoted by $w_i(r)$, and that the additional deflection is denoted by $w(r)$.

In article 2.2, equation (2.2.1), the equation of equilibrium of an element of the plate, when subjected to axisymmetric bending, was given in cylindrical coordinates as

$$\frac{d}{dr}\left[\frac{1}{r}\frac{d}{dr}(r\varphi)\right] = -\frac{Q}{D}$$

The left-side member of this equation is obtained from the expressions for bending moments and since these moments do not depend on the total curvature but only on the change in curvature of the plate, the additional deflection $w(r)$ should be used in this member.

On the other hand, Q being the shear force per unit length normal to the ideal flat initial plate, and not to the actual initial plate, it can be expressed as

$$Q = \sigma_r h(\varphi_i + \varphi)$$

Substitution yields:

$$\frac{d}{dr}\ \frac{1}{r}\frac{d}{dr}\ (r\varphi)\ = -\frac{\sigma_r h}{D}\ (\varphi_i + \varphi) \qquad (2.7.1)$$

This is a non-homogeneous differential equation which has solutions for arbitrary values of σ_r . The physical reason for this fact is that deflections will appear as soon as stresses develop in the plate.

If it is assumed that φ_i is proportional to φ , Eq.(2.7.1) can be written

$$\frac{d}{dr}\left[\frac{1}{r}\frac{d}{dr}\ (r\varphi)\right] = -\frac{\sigma_r h}{D}\ \varphi(1+c)$$

This leads to

$$T_{crit} = T_o(1+c) = T_o\left(1 + \frac{\varphi_i}{\varphi}\right) = T_o\left(1 + \frac{w_{io}}{w_o}\right)$$

or

$$w_o = \frac{w_{io}}{\frac{T_{crit}}{T_o} - 1} \qquad (2.7.2)$$

This expression is similar to the formula giving the deflections of columns.

Equation (2.7.2) can be rewritten in the form

$$w_o = T_{crit}\ \frac{w_o}{T_o} - w_{io}$$

It is clear that if w_o is plotted against w_o/T_o, the result will be a straight line of slope T_{crit}. This is known as the Southwell plot and it provides a method of determining T_{crit} starting from experimental data on T_o as a function of w_o (Fig.32).

When the initial and the buckled shapes are different (i.e., φ_i not proportional to φ) the relationship between w_o and T_o is different and can be derived from energy considerations (see Ref.5), one obtains

$$\frac{T_{crit}}{T_o} = 1 + K_1 \frac{w_{io}}{w_o}$$

or

$$w_o = T_{crit} \frac{w_o}{T_o} - K_1 w_{io}$$

where K_1 is a coefficient depending only on the initial shape.

Again the slope of the straight line resulting from plotting w_o versus w_o/T_o determines T_{crit}.

SECTION III

EXPERIMENTAL METHODS AND RESULTS

3.1 Introduction

Instability is not always characterized by a sudden, clearly distinguishable deflection from the original configuration but rather, in most practical cases, by an increase in the rate of deflection. This is due to imperfections in either the initial configuration, or the application of the load.

The determination of the critical time of instability by means of direct observation is possible only for those configurations in which the ideal conditions are closely attained. This is not the case, unfortunately, for thin plane plates. The initial imperfections of manufacture, the effect of gravity, the perturbations introduced by the attachment of temperature and deflection measuring devices, and perhaps other causes, such as imperfections in the supporting rig, make initial flatness unobtainable in experimental work.

The initial configuration is not flat and consequently deflections appear as soon as the heat is applied and stresses develop in the plate. Nevertheless the critical time of the ideal case can be determined from experimental data if the methods developed in Section II are applied.

The critical temperature can be calculated from data on the temperature distribution by means of the linear theory described in 2.4. This was done in article 2.6 for a particular case.

Another way of determining the critical temperature is by means of the Southwell plot described in 2.7. This method requires data on the relation between the temperature and the deflection at the inner edge of the plate during the process of buckling.

In the following articles a summary is given of the methods applied or developed in this research effort for the gathering of data on temperature and deflections; the tests performed are described and the data obtained are used to determine the critical temperature by means of a Southwell plot. Finally the results are compared with the predictions of the previously obtained formulas.

3.2 Measurement of the Lateral Deflections

The selection of a displacement measuring device for a particular experiment should depend upon a number of considerations relating to the specific characteristics of that experiment. Perhaps the most important consideration is the order of magnitude of the displacements to be measured.

In our particular case we are interested in corroborating theoretical results obtained from the linear theory on the deflection of thin plates. Consequently we are concerned with deflections smaller than the thickness of the plate.

Since the plate specimens tested in our experiments had a thickness of $h = 0.058$ in., we required a device capable of measuring with reasonable accuracy displacements in the range from 0 to 50 thousandths of an inch.

The criterion of what can be considered a reasonable accuracy is the degree of precision required in the determination of the critical temperature. In an average test it was found that an absolute error in the temperature reading of $\pm 2^{\circ}F$ and an absolute error in the central deflection reading of 0.001 in. result in a relative error of 8 per cent in the value of the critical temperature as calculated by the Southwell plot. This is considered acceptable.

Thus the requirements are a usable range from 0 to 50 thousandths of an inch with an absolute error smaller than one thousandth of an inch.

These are not hard requirements to fulfill and, as a matter of fact, a regular dial-gauge satisfies them. Nevertheless, other considerations rule out the use of dial gauges in favor of an optical system.

The advantages of an optical system are various; two of them are of particular importance:

(a) An optical system does not interfere with the phenomena, and

(b) it provides a direct picture of the deflection pattern all over the plate.

The optical system of deflection measurement selected for our experiments is schematically shown in Fig.12. A parallel beam of rays of light carrying the image of a grid of straight lines parallel to the plane xz (the plane xz is determined by the normal to the plate and the direction of incident light) is projected on the surface of the specimen, which has a mirror finish, and is reflected by the specimen on an observation milk glass G parallel to the plane of the specimen. Thus an image is formed on the milk glass.

When the plate is flat the image of the straight line abc is a straight line $a_1b_1c_1$. If it is assumed that the plate is fixed at its outer edge, the slopes of the elements a' and c' will not change when the plate deflects and consequently their images a_1 and c_1 will not move.

Let us consider now the element b' on the axis Oy. The normal to this element, in the initial flat state, is n_1 in the plane yz. If the deflections of the plate are axisymmetrical, the element b' will deflect to a position such as b_2' and its normal will be n_2 in the plane yz. Thus the angle φ between n_1 and n_2 is equal to the change in radial slope of the element b' and the image of b_2' will be a certain point b_2.

If the deflection w of the element b' is neglected compared with the distance d between the planes of the plate and the observation glass, it follows from elementary optics and geometry that

$$\tan \varphi \simeq \varphi = \frac{D}{2d} \qquad (3.2.1)$$

where D is the distance $\overline{b_1b_2}$, that is the central distortion in the direction parallel to Oy of the image of the line abc.

The photographs of Figs.13 and 14 show how the image of the grid of lines appears for the plate in the flat state and in the deflected state. The images corresponding to an improved grid are given in Fig.15.

By comparison of two photographs corresponding to the initial and the deflected states the image displacements D of a number of points on the diameter Oy can be measured and the corresponding changes in slope can be calculated. Thus the function $\varphi(r) = dw/dr$ can be plotted and by integration the deflection of any point will be given by

$$w(r) = \int_b^r \varphi dr = \frac{1}{2d} \int_b^r D dr \qquad (3.2.2)$$

3.2.1 The Moiré Technique

The image distortion D can be magnified, if necessary, by means of the so-called Moiré fringe technique. This technique is widely known and has been the subject of a number of papers some of which are listed under the references.

Basically the method consists in superimposing on the image of a grid of lines (usually parallel lines either marked on the surface of the model to be studied or reflected by its surface on an observation screen, as in our case) another analogous grid of lines, slightly rotated with respect to the former one, so as to produce a so-called mechanical interference resulting in fringes which look somewhat like the textile material known as Moiré (from here the name of the phenomenon).

When the model is unloaded the image of the projected grid of lines appears as an array of parallel straight lines (Fig.16), and superposition on this image of an analogous grid, slightly rotated (Fig.17) results in a Moiré pattern with straight fringes (Fig.18).

When the model is loaded the image of the projected grid appears distorted (Fig.19) and superposition of the interfering grid results in a Moiré pattern of curved fringes (Fig.20).

If the relative rotation of the two grids is small, small distortions of the projected image result in large distortions of the Moire pattern.

In the experiments conducted in this research effort the distortions D of the projected image were large enough to be measured directly and consequently no use was made of the Moiré technique in the calculation of the deflections. The interpretation of the distortion of the Moiré pattern is included in Appendix A. It was felt that the complications involved in the calculation of the distortions D by interpretation of the Moiré pattern were not justified, as a direct reading of D from an enlarged view of the image obtained in an Optical Comparator was sufficiently accurate. Nevertheless, from the qualitative point of view, the Moiré technique proved to be very satisfactory for direct observation of imperfections in the initial flatness of the plates, as well as for the observation of the rate of deflection during the buckling phenomenon.

Thus it was decided to use the Moiré technique in half of the image, for qualitative observation, leaving the other half as direct image, for quantitative determination of the deflections.

The resulting composite image is shown in Figs.21 and 22. Figure 21 corresponds to the initial state, the upper half being a direct image as reflected by the plate and the lower part a fringe pattern obtained by the Moiré technique. Fig.22 is the image in the buckled state.

The semicircles appearing on the direct image serve to check the axisymmetry of the deflected mode.

3.3 Description of the Test Rig

The test rig is sketched in Fig.23 and photographed in Figs.24 and 25. It consists of an optical bench on which a 300 watt concentrated arc lamp provides a light source of high brilliance and small size. The light, after being projected through the target, is converted by

means of a suitable set of lenses into a parallel beam of light large enough to cover the whole surface of the plate to be tested. A mirror reflects the beam of light on the plate which is mounted horizontally on a massive support (Fig.26). The highly polished surface of the plate reflects the light onto an observation milk glass where the image is formed. The observation mirror situated above the milk glass is only for convenience of observation.

The temperature distribution over the plate is recorded by means of chromel-alumel thermocouples attached to the lower surface of the specimen. The axisymmetric character of the heating is also checked.

The heating unit (Fig.27) was designed so as to approach as closely as possible the conditions of radial heating. The heater consists of a resistance wire element laid on a support of asbestos. When mounted on the plate its two halves clamp on the inner edge of the plate, slightly overlapping it. The heater weighs only two ounces and moves with the plate during the process of buckling.

The specimens used in the tests were annular plates with the following characteristics:

Material: steel

Poisson ratio: $\nu = 0.25$

Coefficient of thermal expansion: $\alpha = 6.1 \times 10^{-6}\ {}^{o}_{F}{}^{-1}$

Inner radius: $a = 1.5$ in.

Outer effective radius: $b = 5$ in.

Thickness: $h = 0.058$ in.

The front surface of the specimens was polished to a mirror finish.

3.4 Buckling Tests

Three tests were conducted for different values of the heat flux. The changes in the heat flux were obtained by means of a variable rheostat in series with the heating unit.

A continuous record of the temperature distribution was obtained and a simultaneous sequence of pictures was taken of the image during the heating process.

The sequence of images obtained during test no.1 is shown in Fig.28. The photographs correspond to 0, 30, 61, 90, 120, 150 and 180 seconds respectively.

By comparing these photographs with a picture of the image as reflected by a calibration flat mirror, the displacements D (proportional to the change in slope) can be determined. This can be done with great accuracy in an optical comparator.

In this manner the change in slope distribution over the radius can be plotted for the recorded intervals of time. This has been done in Fig.29 for test no.1. In this plot θ is the slope in the radial direction and K is a constant which includes the factor 1/2d (see Eq.(3.2.1)) and the magnification factor of the optical comparator. Integration of these curves yields the deflections.

As mentioned before, in this particular test the images were compared with those of a flat calibration mirror. Consequently, the slopes rather than the changes in slope, were obtained for every point. It can be seen that for $t = 0$ the central deflection appears to be $w_{io} = 3.76$ thousandths of an inch.

The variation of the total central deflection $w_{io} + w_o$ with time is shown in Fig.30. Actually, for the purpose of determining the critical temperature by means of the Southwell plot, the determination w_{io} is not required. In tests 2 and 3, the images of the plate for the successive intervals were compared with the image of the initial state ($t = 0$). In this manner the changes in slope are directly determined and the corresponding increments in the deflection can be calculated.

In Fig.31, corresponding to test no.1, the edge temperature increment T_o and the central deflection increment w_o are plotted against time. From these data a Southwell plot can be made. This is

done in Fig.32 where one can see that the Southwell line is straight in the small deflection region. It determines the value

$$\left(T_{crit}\right)_1 = 127^{\circ}F$$

Tests 2 and 3 were conducted in the same manner (see Figs.33, 34, 35, 36 and 37) resulting in the following critical temperatures:

$$\left(T_{crit}\right)_2 = 120^{\circ}F$$

$$\left(T_{crit}\right)_3 = 111^{\circ}F$$

For the purpose of comparison, these results were plotted in Fig.11 which summarizes the results of both theory and experiment.

APPENDIX A

INTERPRETATION OF THE DISTORTIONS IN THE INTERFERENCE FRINGES OBTAINED BY THE MOIRÉ TECHNIQUE

The nature of the Moiré interference pattern can be better understood by observation of the phenomenon on a magnified scale. In Fig.A-1 it can be seen that the direction and location of the black interference fringes correspond to those of lines such as $\underline{a}$ along which there is total coverage of light.

If the interfering grids are schematically represented by thin lines (Fig.A-2), the location of the black interference fringes is determined by the middle points of the segments between intersection points.

Using this schematic representation Fig.A-3 has been constructed.

Let a_1 and a_2 be two consecutive lines of the image projected by the specimen in the initial state, and let b be one line of the fixed interfering grid.

If A is the middle point of the segment determined by the intersection of b with a_1 and a_2, there will be, in the initial state, a certain fringe f passing through the point A.

When the specimen deflects, the lines a_1 and a_2 become a_1' and a_2' and the point A moves along the line b to the point A', the fringe f becoming f'.

The displacement D of the point P can then be obtained from reading the distance $AA' = \delta$

$$D = \delta \sin \alpha \simeq \delta\alpha$$

where α is the angle formed by the grids.

Nevertheless, as it was discussed in 3.2, the displacement D is proportional to the change in radial slope only when P is on the diameter Oy and the deflection is axisymmetric.

The displacement D of points P that are not on the axis Oy determines only one component of the maximum slope of the element corresponding to point P .

To obtain readings of D corresponding to points P on the axis Oy only the points A' lying on Oy can be considered.

In our case it was found that the number of fringes that intersected the axis Oy was not sufficient to obtain a satisfactory determination of the distribution of change in slope along Oy .

In conclusion it was decided that the Moiré technique was satisfactory only for qualitative observation while the method of direct image as explained in 3.2 was more reliable and useful for the quantitative estimation of the changes in slope of the plate.

REFERENCES

1. Carslaw, H. S., and Jaeger, J. C., Conduction of Heat in Solids, Oxford, Clarendon Press, 1959, pp. 332-334.

2. Timoshenko S., and Woinowsky-Krieger, S., Theory of Plates and Shells, McGraw-Hill Book Co., 1959, p.53, eq.56.

3. Timoshenko S., and Goodier, J. N., Theory of Elasticity, McGraw-Hill Book Co., 1951, pp.406-407, eq.(i).

4. Hildebrand, F. B., Advanced Calculus for Engineers, Prentice-Hall, Inc., 1958, Section 5.5, p.218.

5. Queinec, A., Thermal Buckling of Centrally Heated Circular Plates, SUDAER No.106, Stanford, June 1961.

6. Duncan, J. P., and Brown, C. J. E., Determination of Slope Contours in Flexed Elastic Plates by the Salet-Ikeda Technique, 1961, Society for Experimental Stress Analysis Paper No.671.

7. Ligtenberg, F. K., The Moiré Method - a New Experimental Method for the Determination of Moments in Small Slab Models, 1955, Proceedings of the Society for Experimental Stress Analysis, Vol.XII, No.2, pp.83-98.

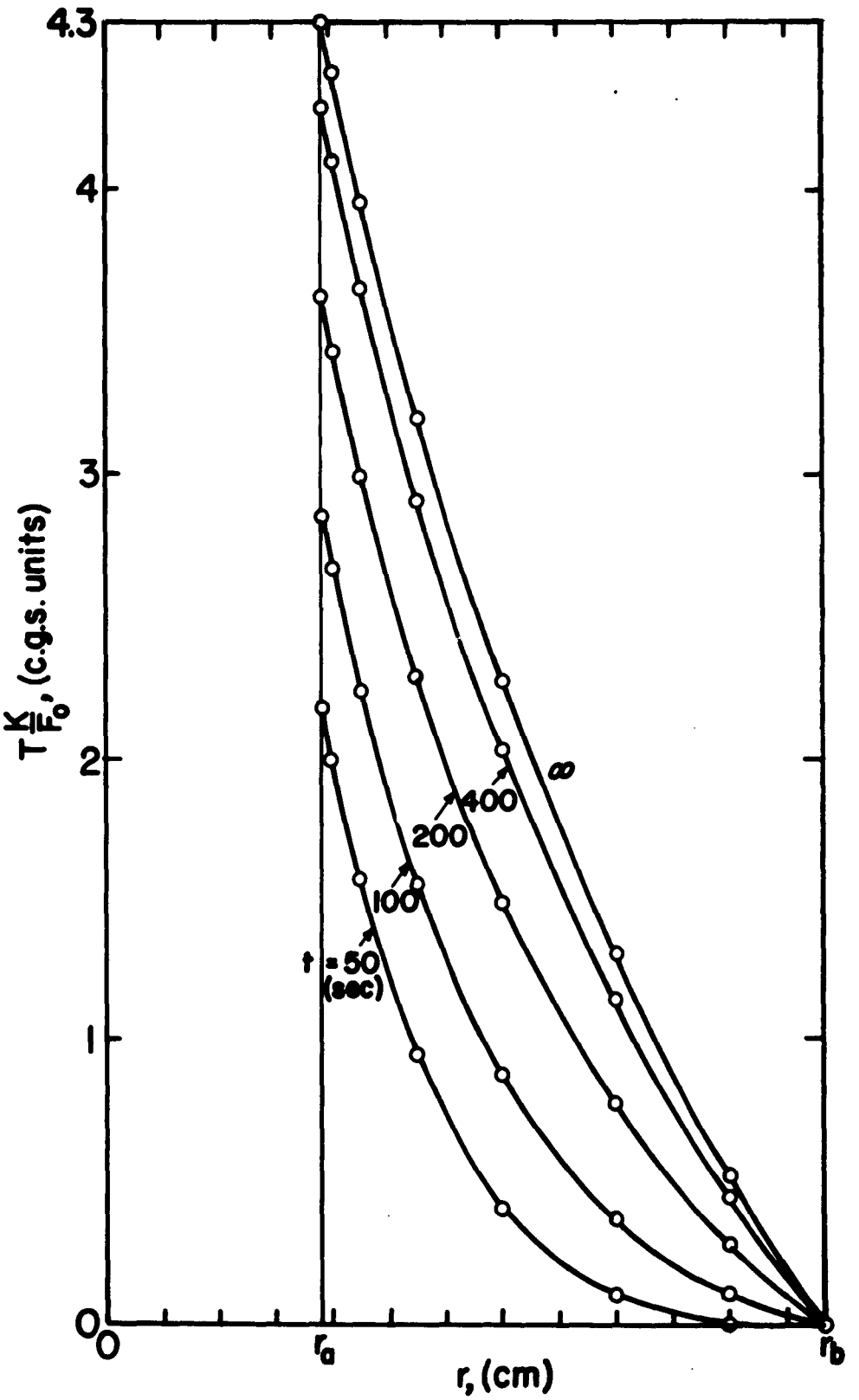

Fig.1. Temperature Distribution from Theory Assuming no Heat Dissipation to the Environment

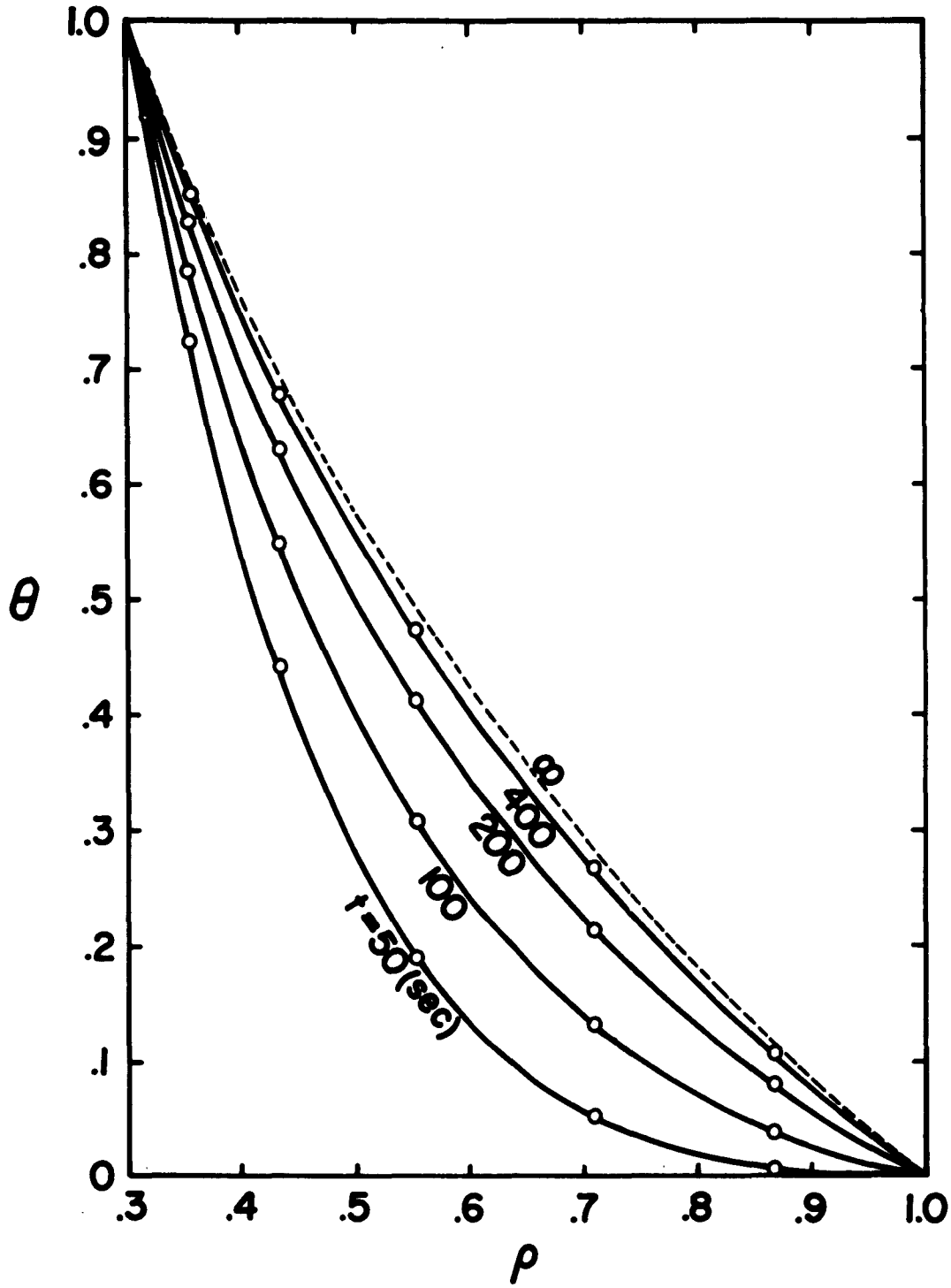

Fig.2. Nondimensional Temperature Distribution
(Theory - no Heat Dissipation)

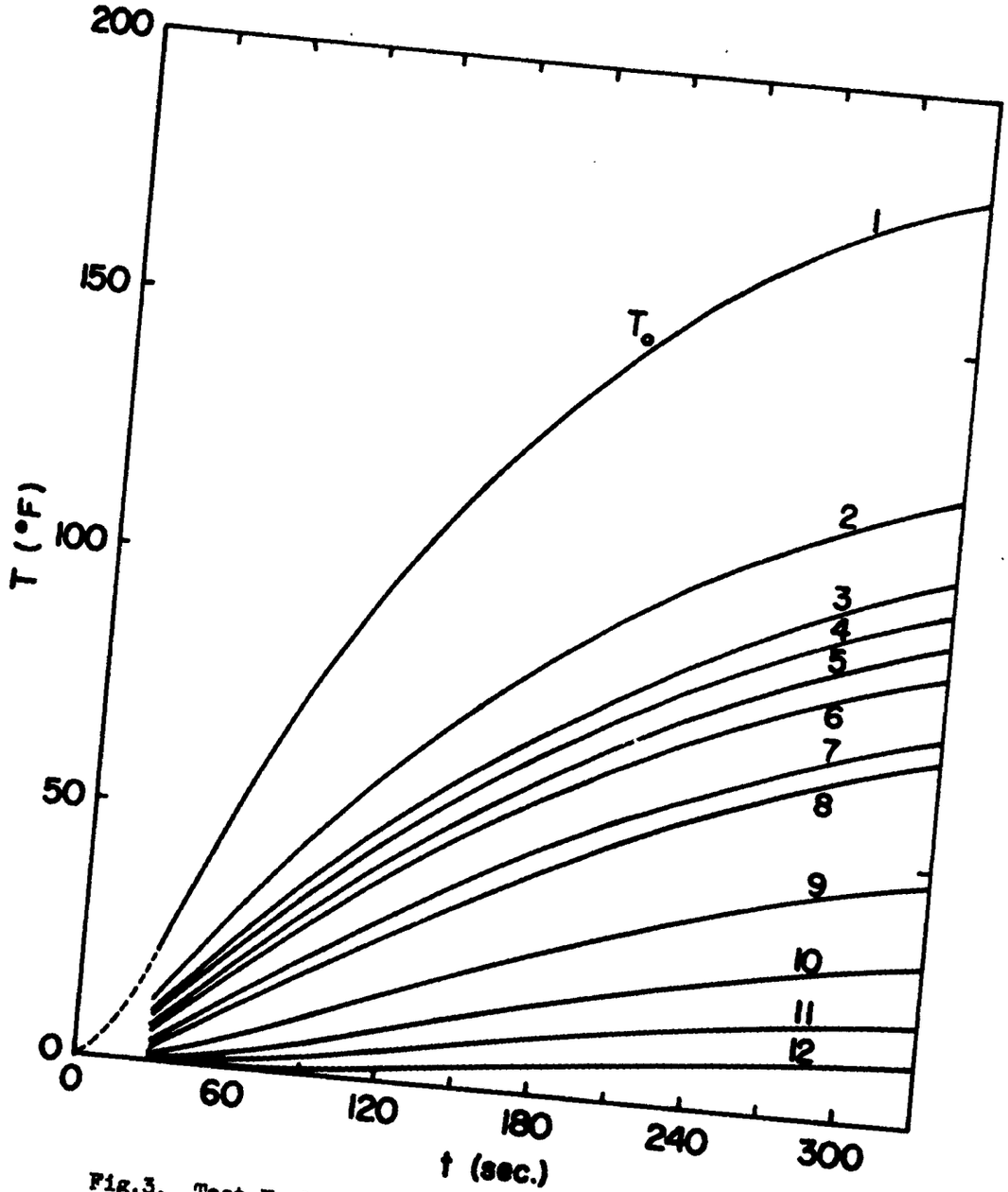

Fig.3. Test No.1 - Temperature Variation with Time

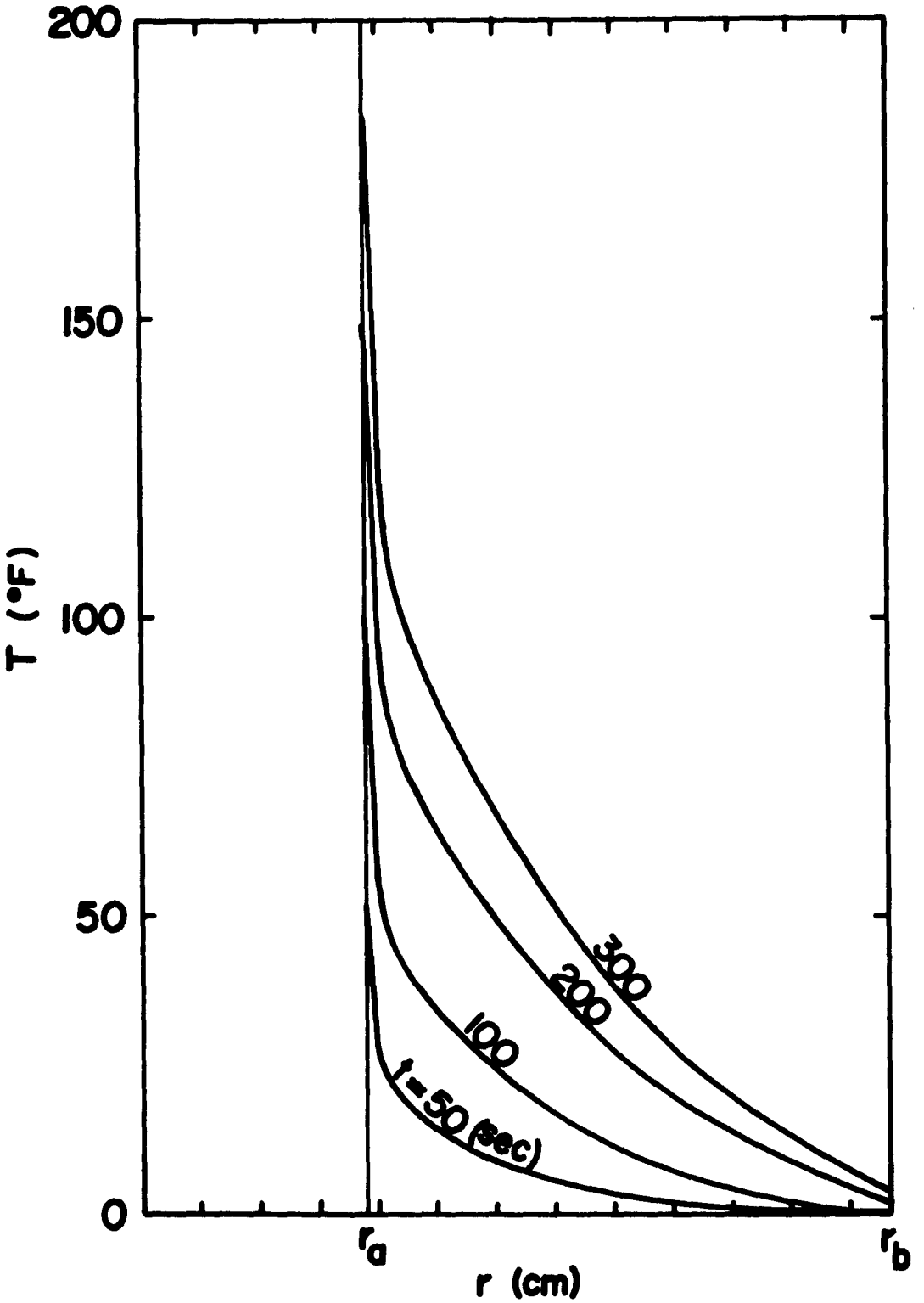

Fig.4. Test No.1 - Temperature Distribution over the Plate

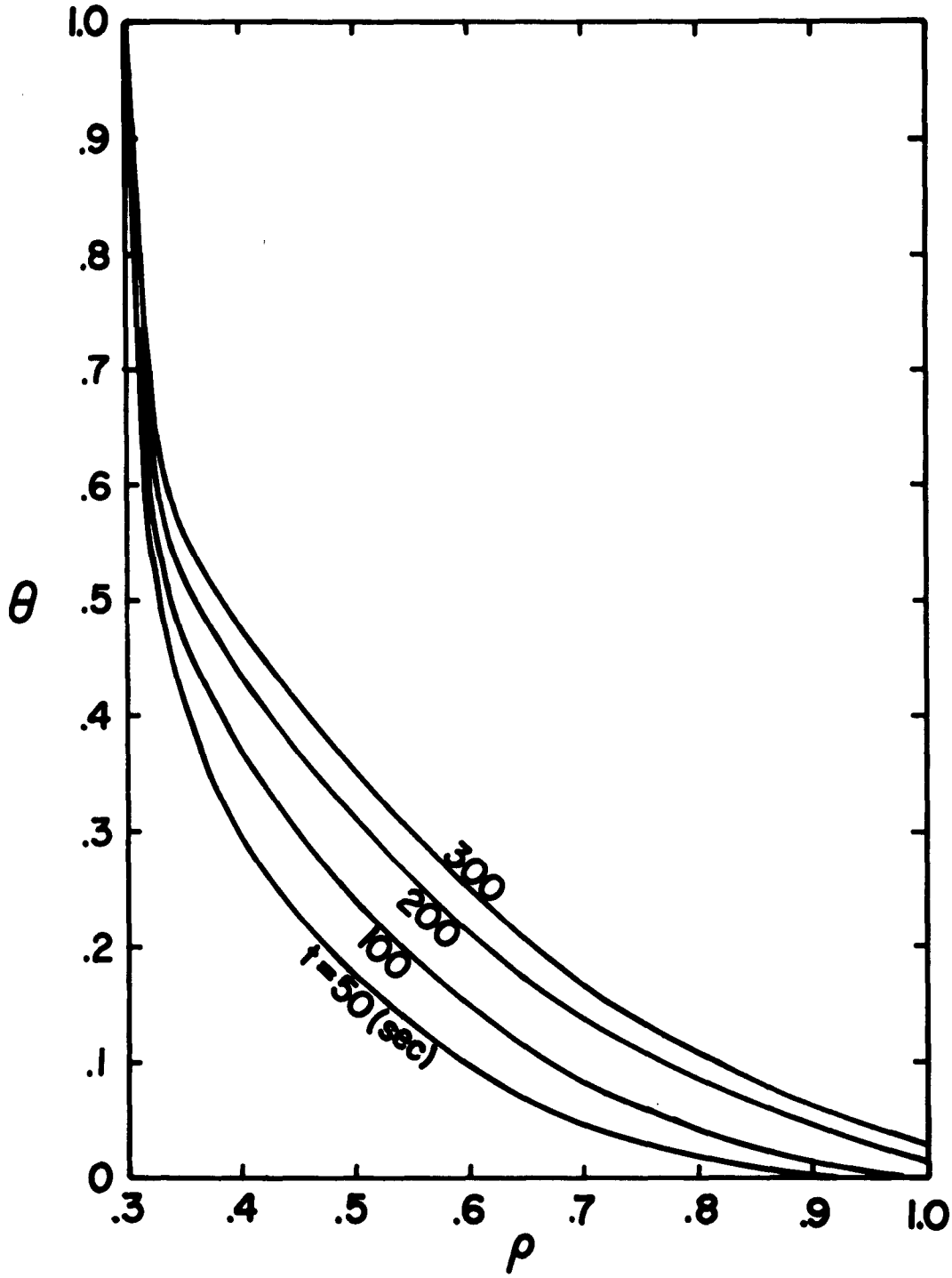

Fig.5. Test No.1 - Nondimensional Temperature Distribution

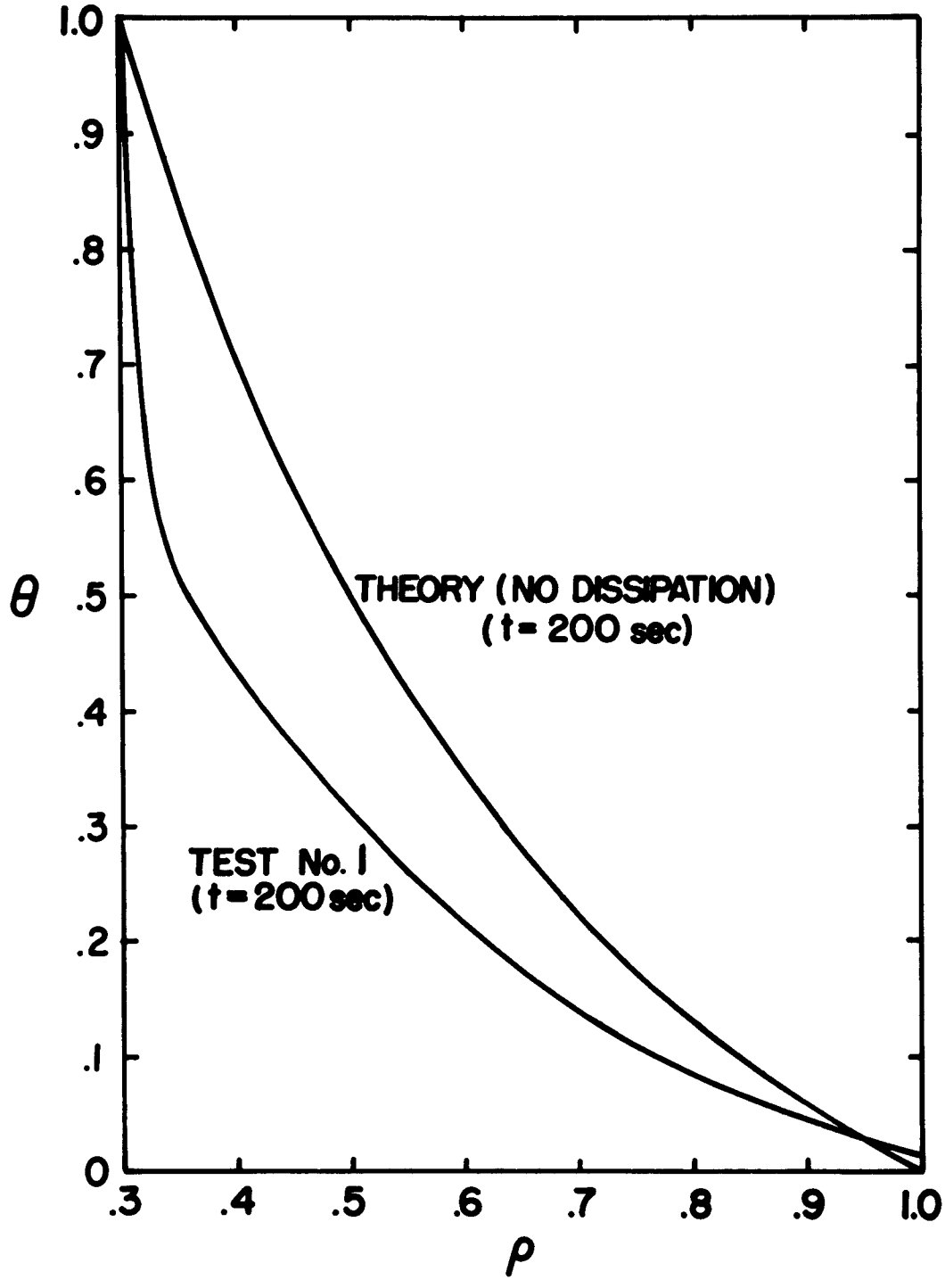

Fig.6. Nondimensional Temperature Distribution (Comparison)

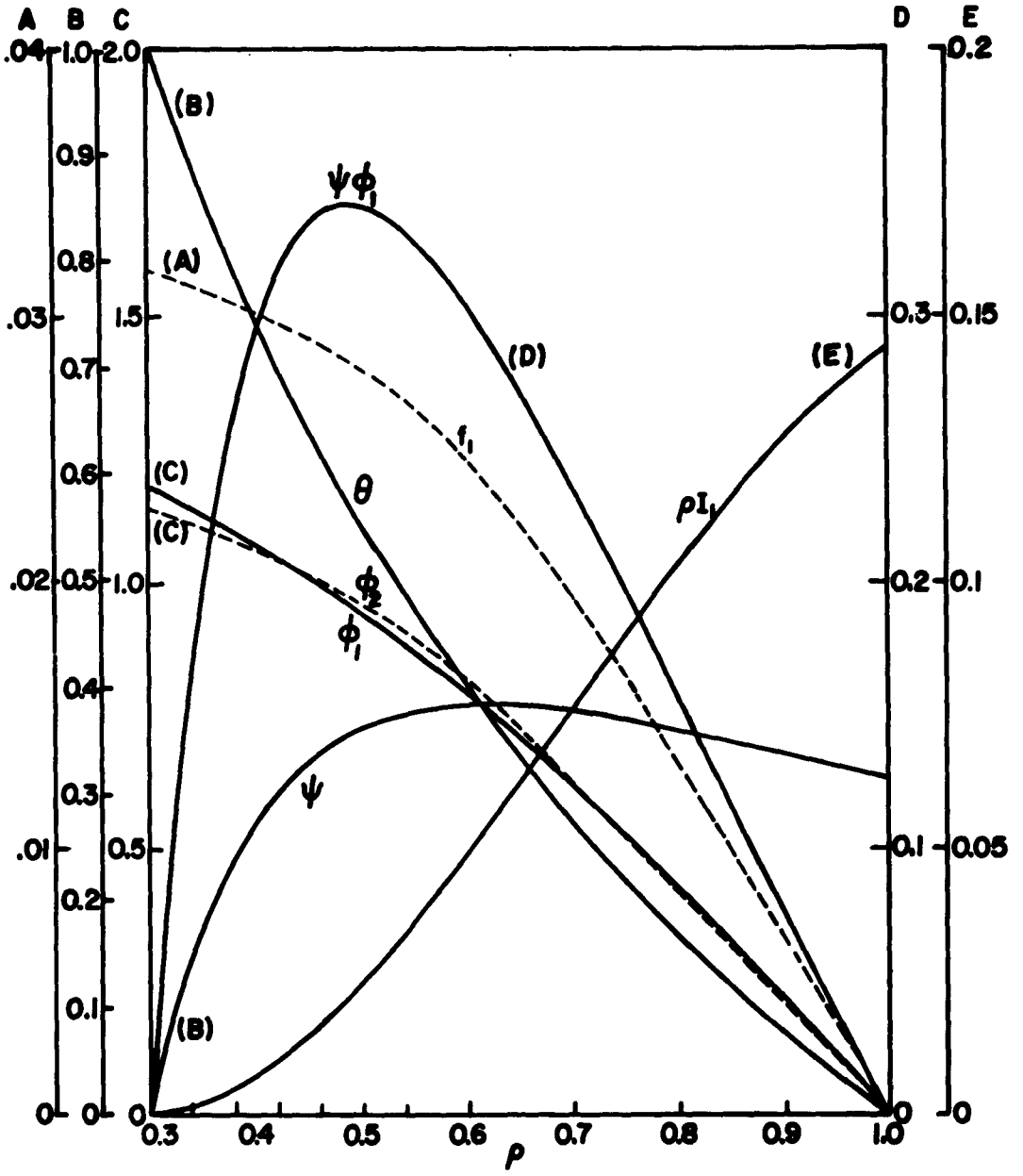

Fig.7. Stodola-Vianello Method. Graphical Integration

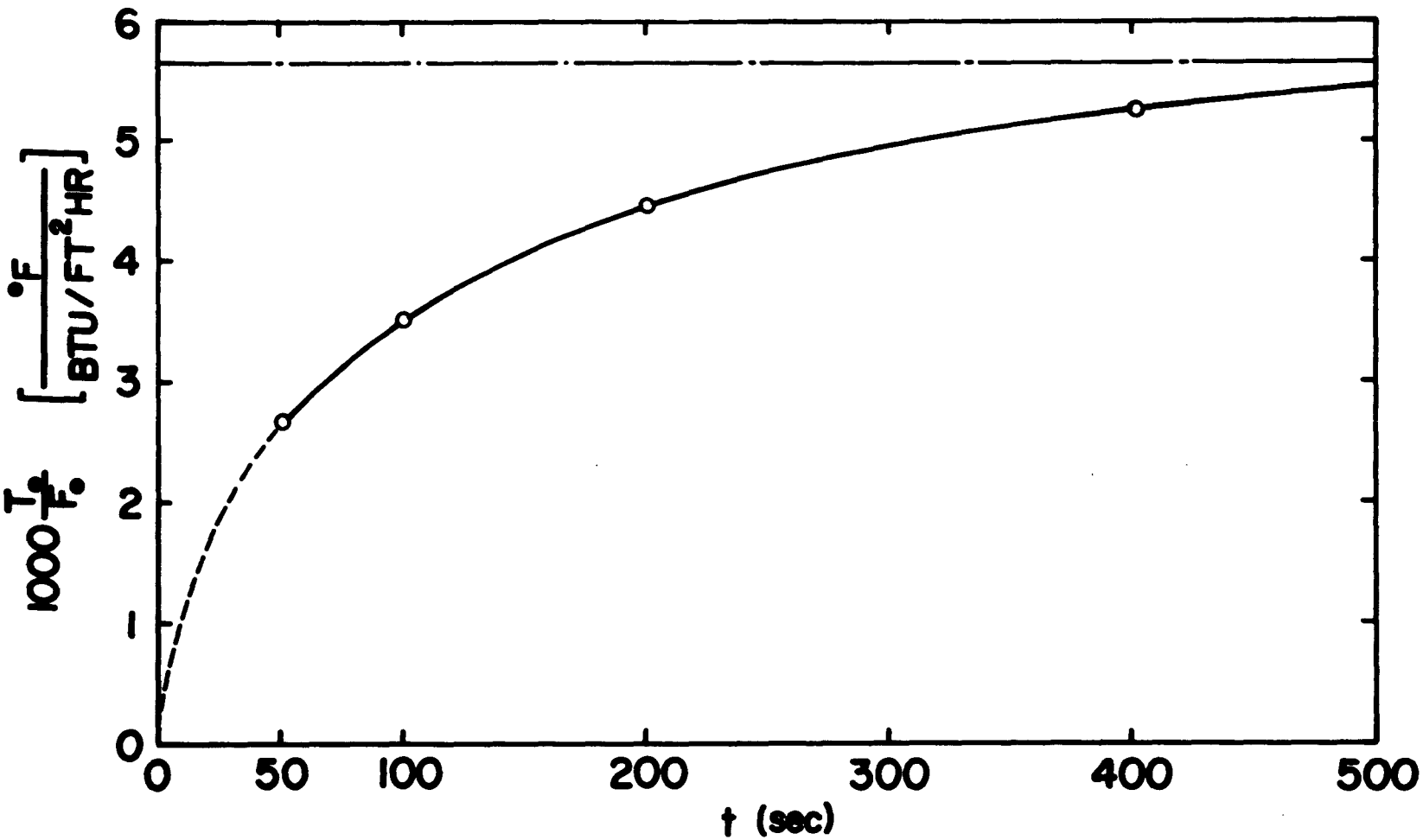

Fig.8. Edge Temperature Variation with Time (Theory - no Heat Dissipation)

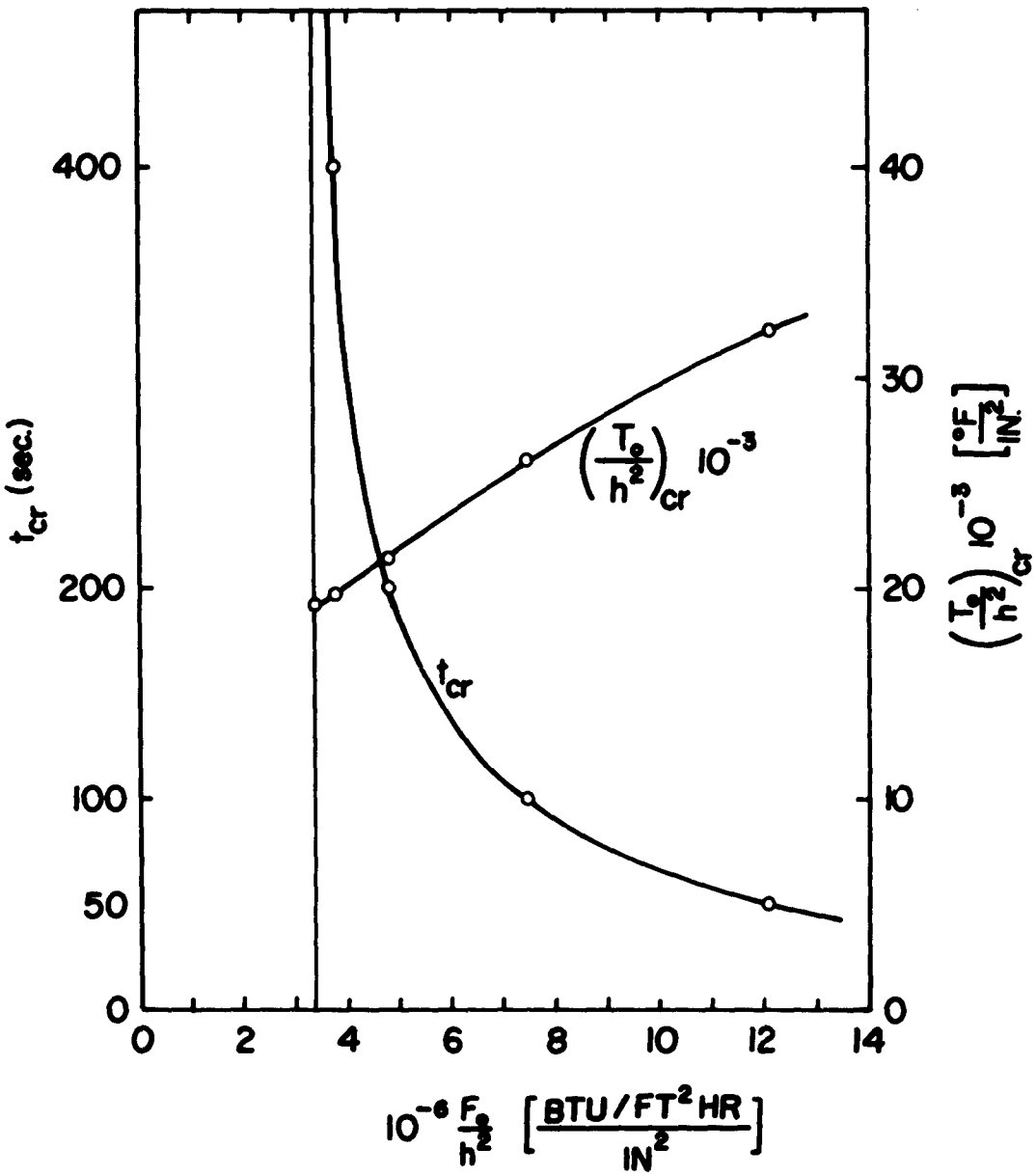

Fig.9. Critical Edge Temperature $(T_o/h^2)_{crit}$ and Critical Time versus Heat Input Flux (Theory - no Heat Dissipation)

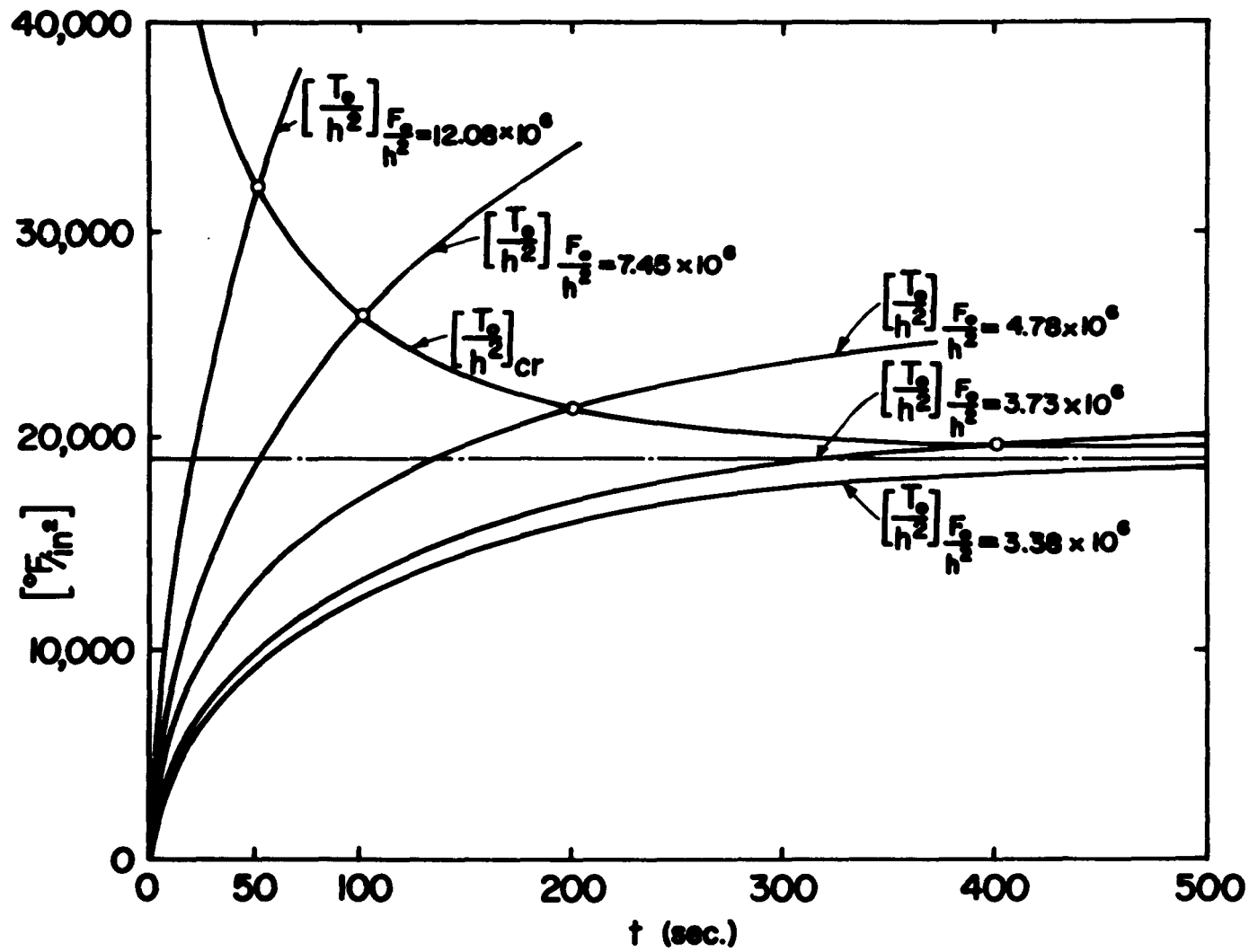

Fig.10. $(T_o/h^2)_{crit}$ and (T_o/h^2) versus Time (Theory - no Heat Dissipation)

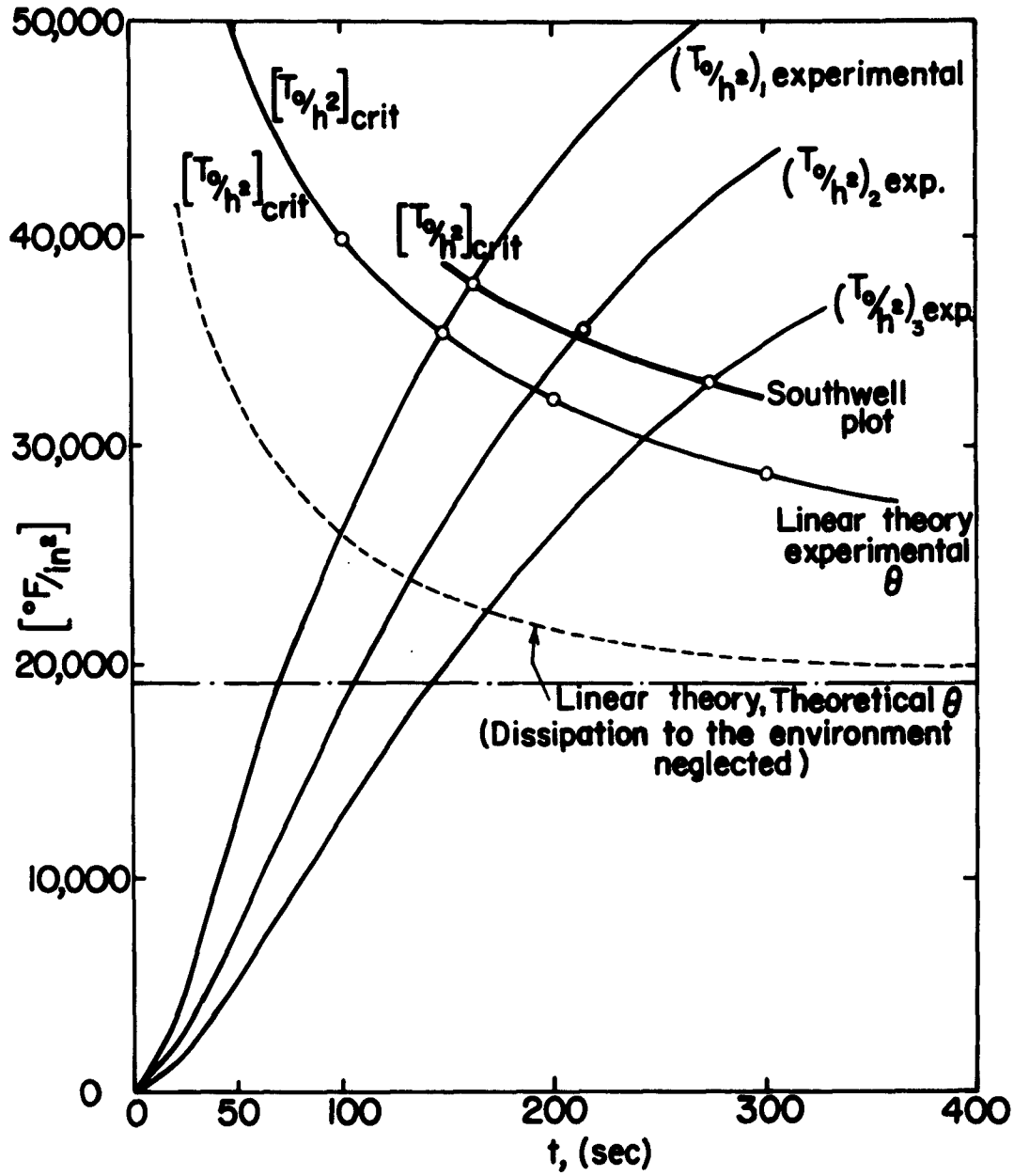

Fig.11. $(T_o/h^2)_{crit}$ versus Time; and (T_o/h^2) for Tests Nos.1, 2 and 3

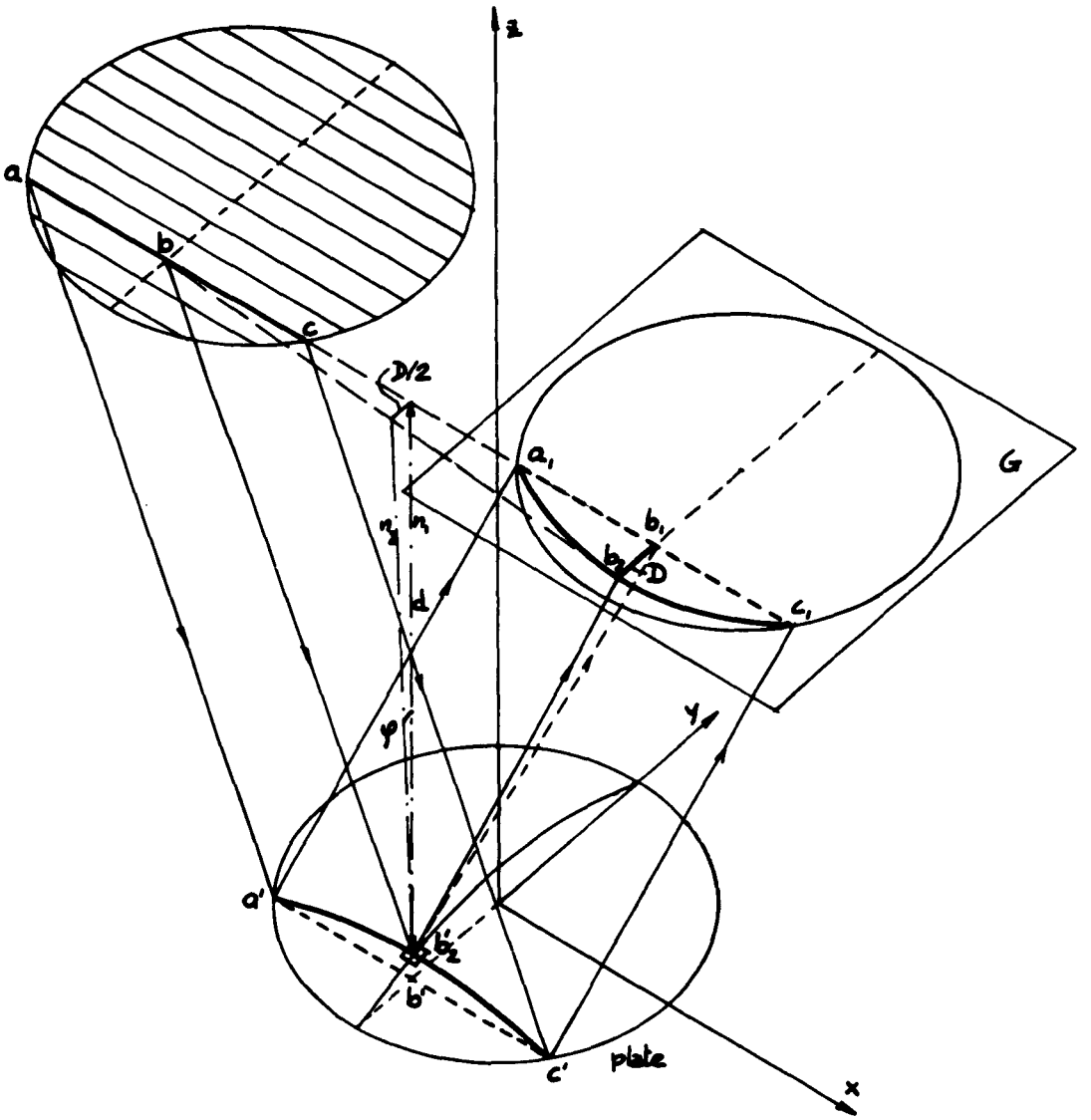

Fig.12. Optical Method of Measurement of the Changes in Radial Slope

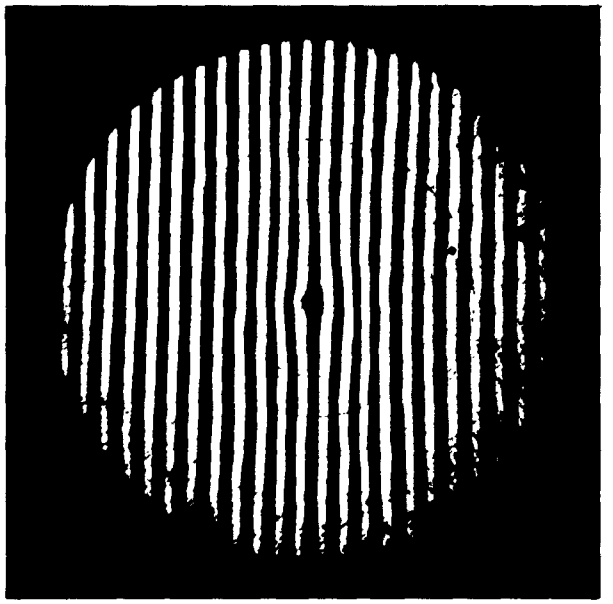

Fig.13. Image of Unloaded Plate

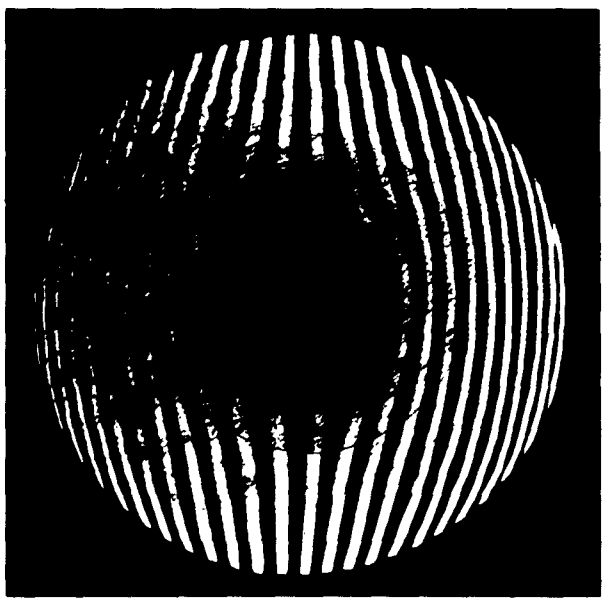

Fig.14. Image of Loaded Plate

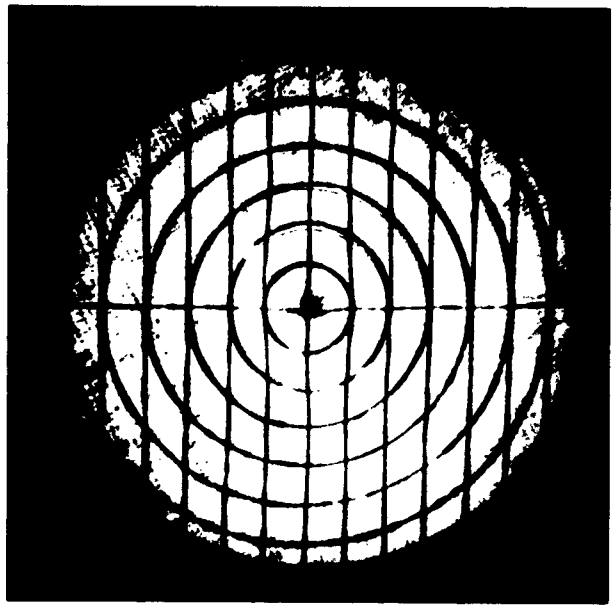

Fig.15. (a) Image of Unloaded Plate

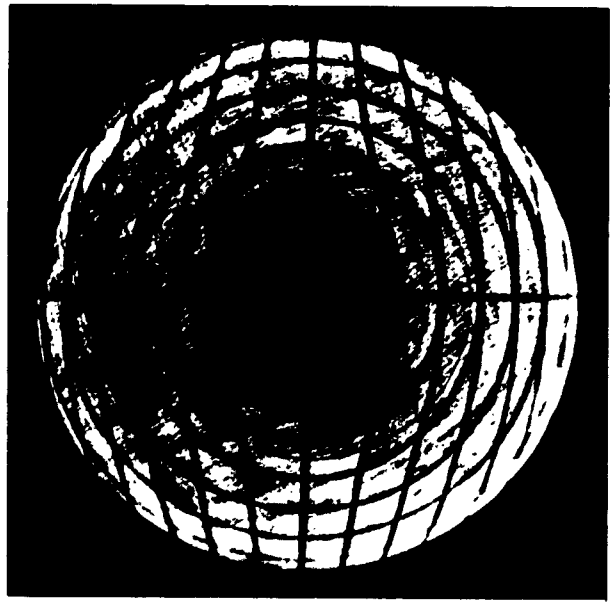

Fig.15. (b) Image of Loaded Plate

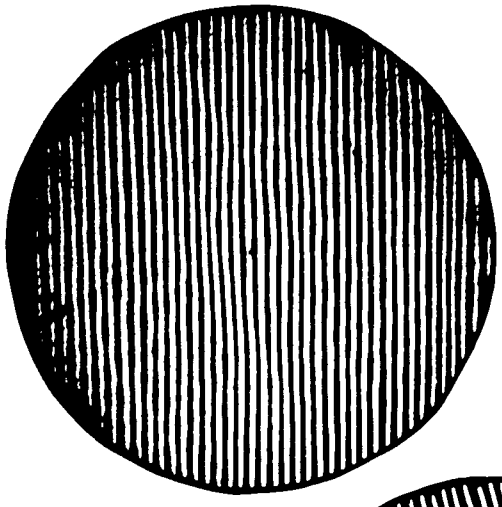

Fig.16. Image of Unloaded Plate

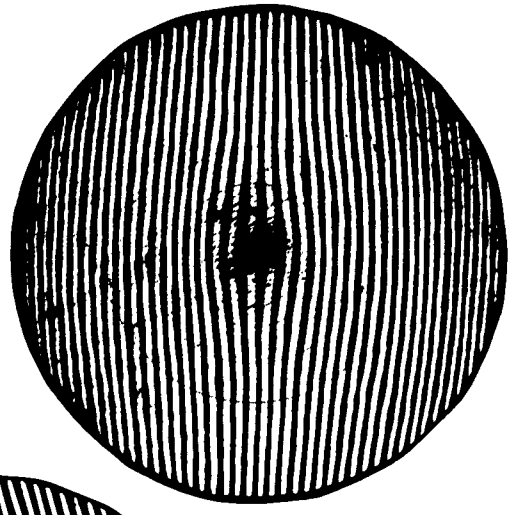

Fig.19. Image of Loaded Plate

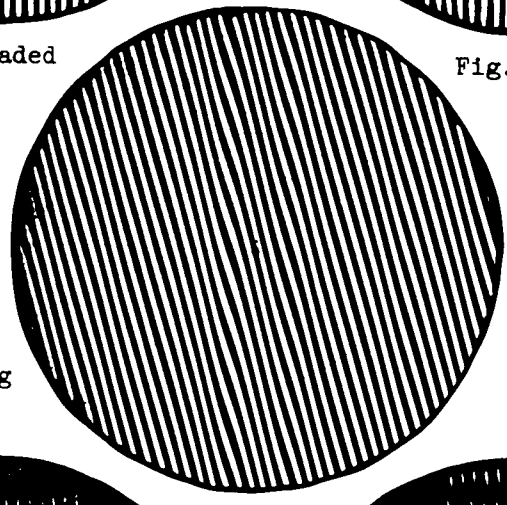

Fig.17. Interfering Grid

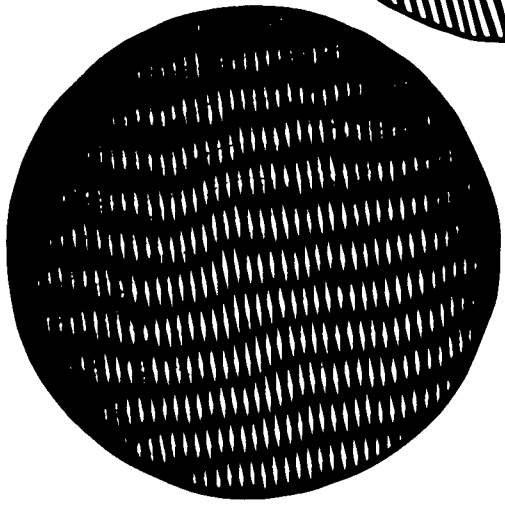

Fig.18. Moire Fringes of Unloaded Plate

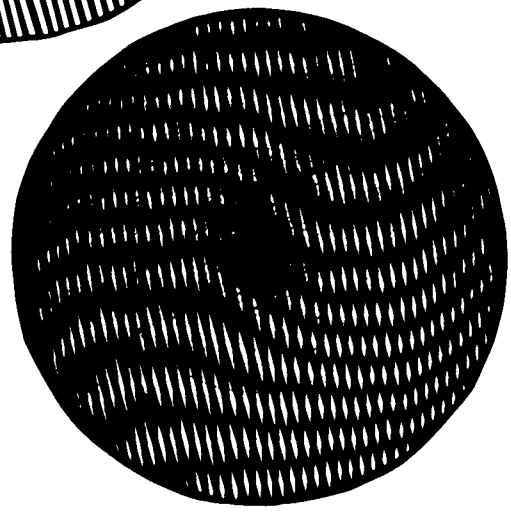

Fig.20. Moire Fringes of Loaded Plate

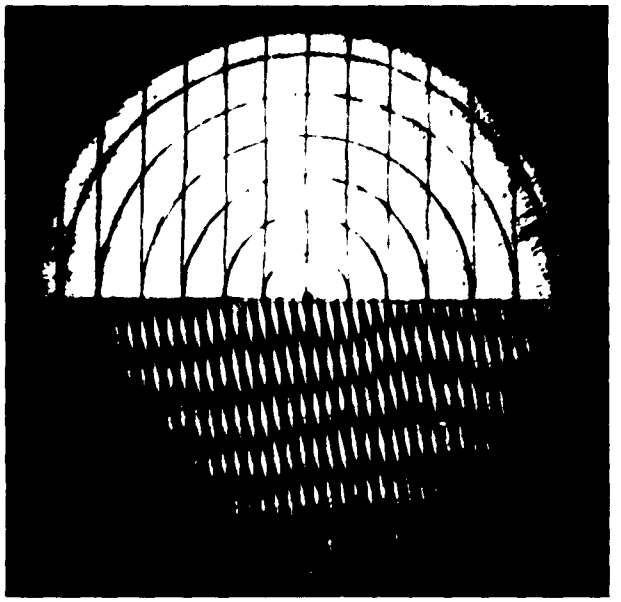

Fig.21. Image of Unloaded Plate

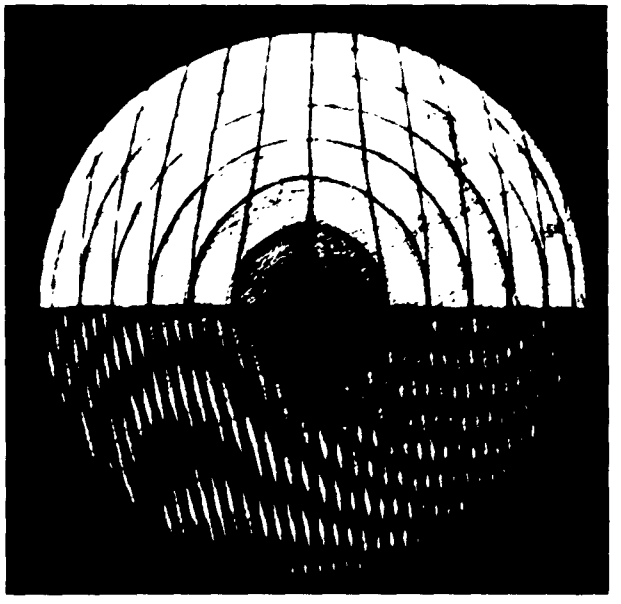

Fig.22. Image of Loaded Plate

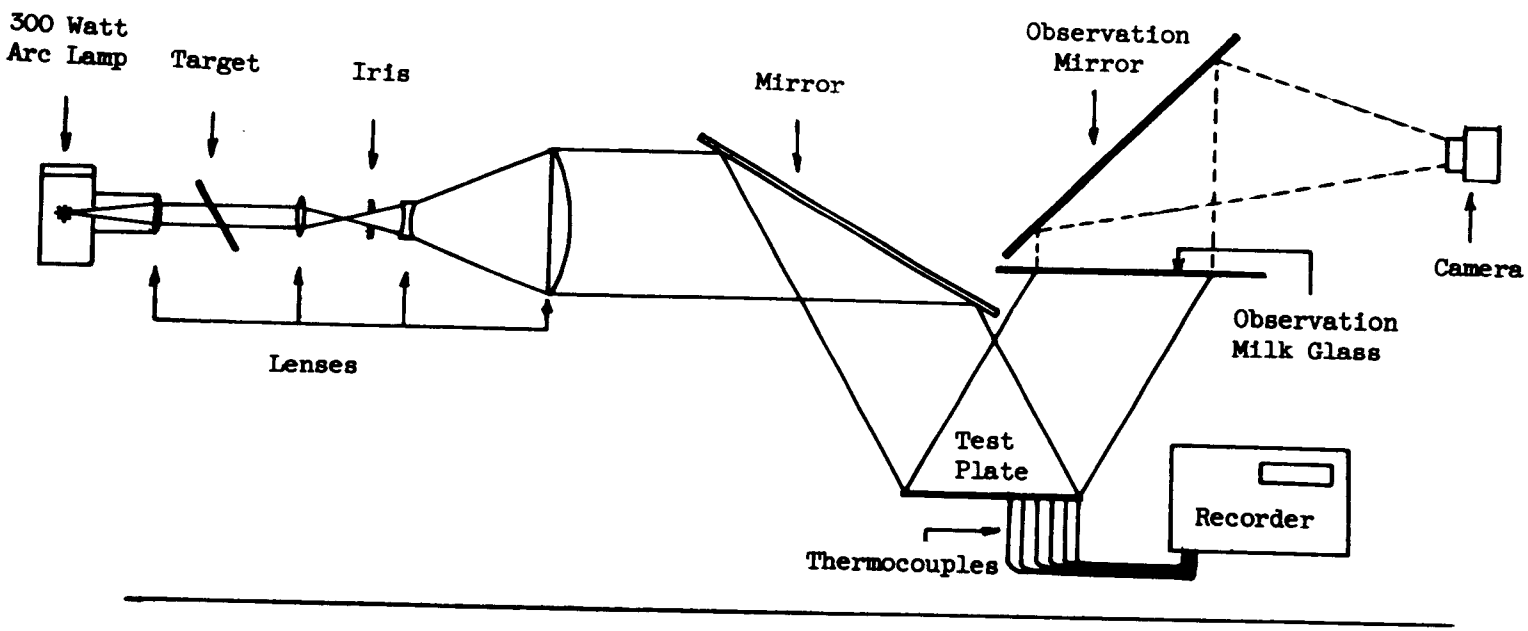

Fig.23. Test Rig

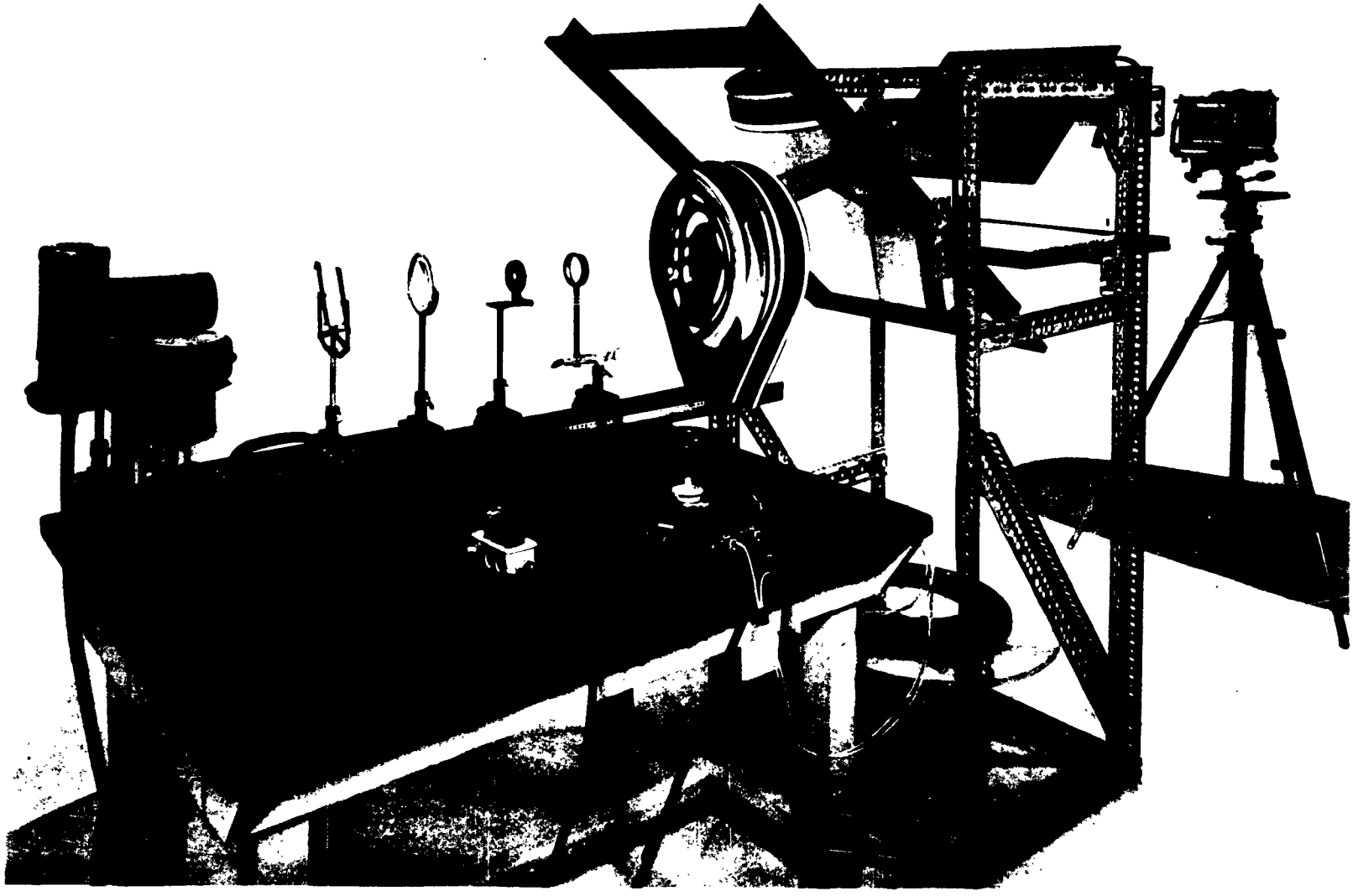

Fig.24. Test Rig

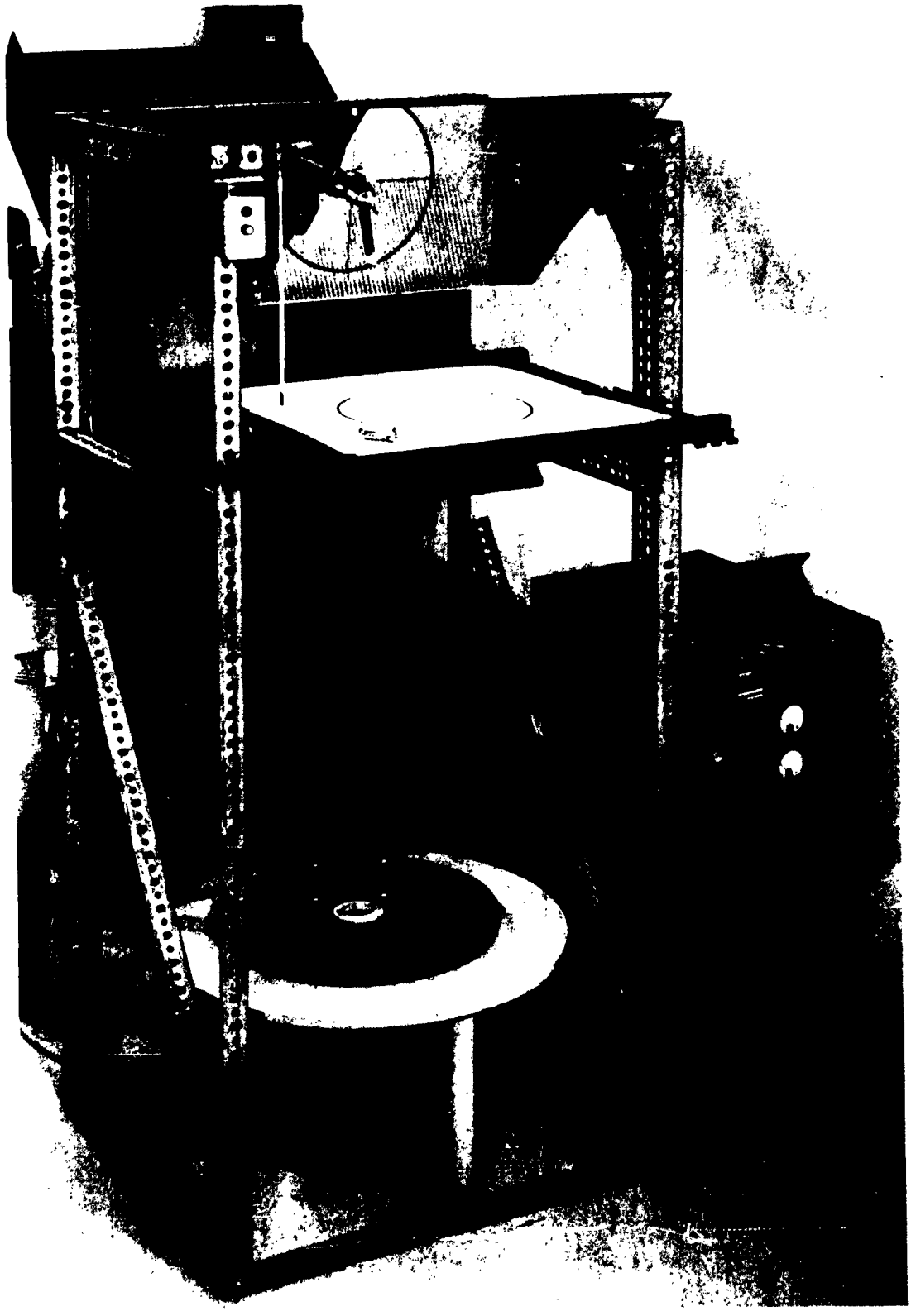

Fig.25. Test Rig

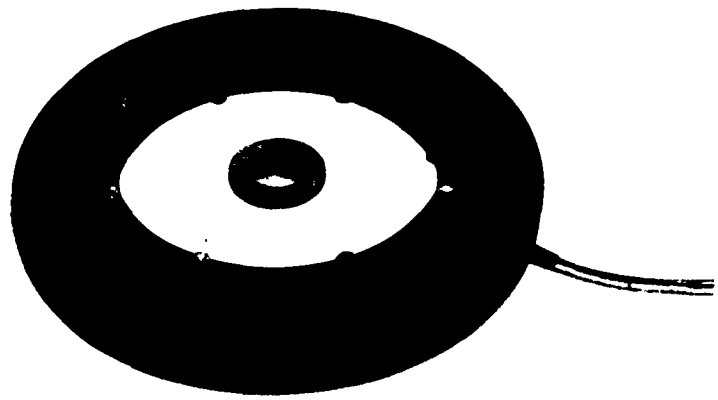

Fig.26. Plate Mounted on its Support

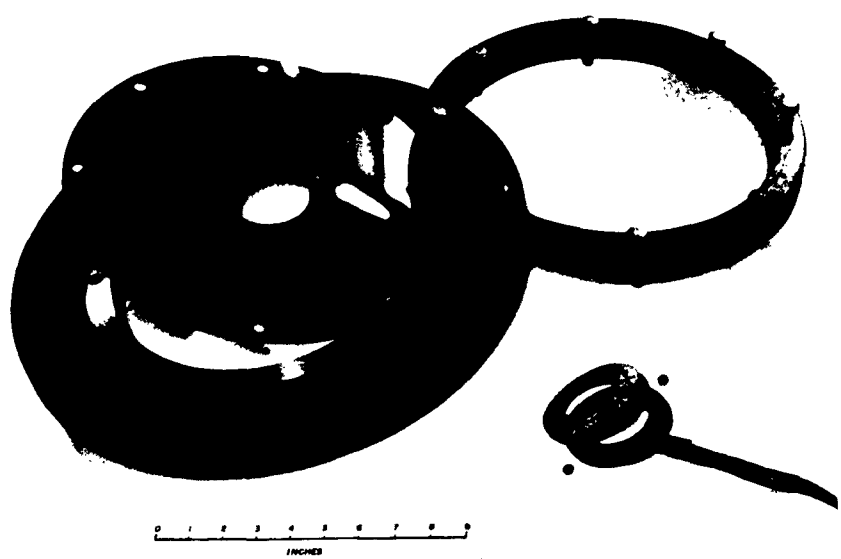

Fig.27. Plate, Support and Heater

t = 0
w = 0

t = 30 sec
w = 0.76×10^{-3} in.

t = 61 sec
w = 2.57×10^{-3} in.

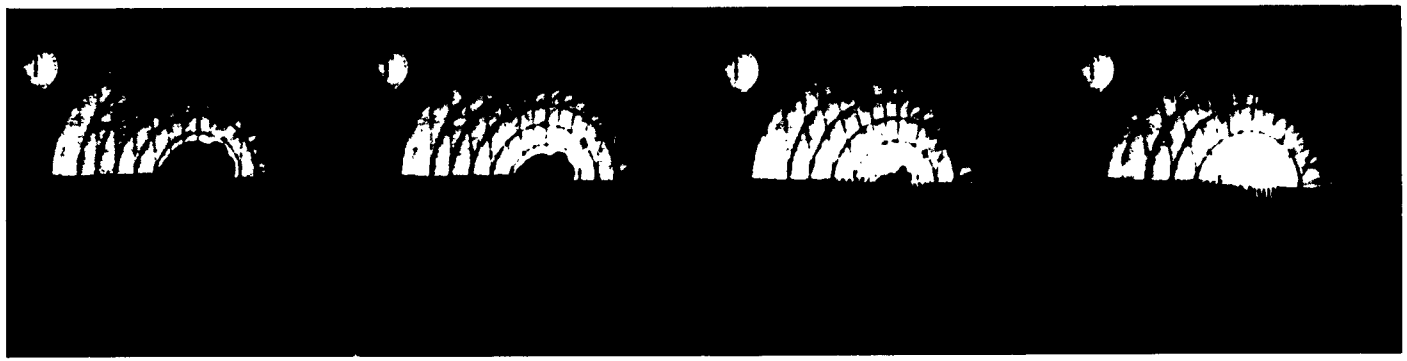

t = 90 sec
w = 6.37×10^{-3} in.

t = 120 sec.
w = 16.40×10^{-3} in.

t = 150 sec
w = 32.94×10^{-3} in.

t = 180 sec
w = 47.64×10^{-3} in.

Fig.28. Test No.1 - Sequence of Images

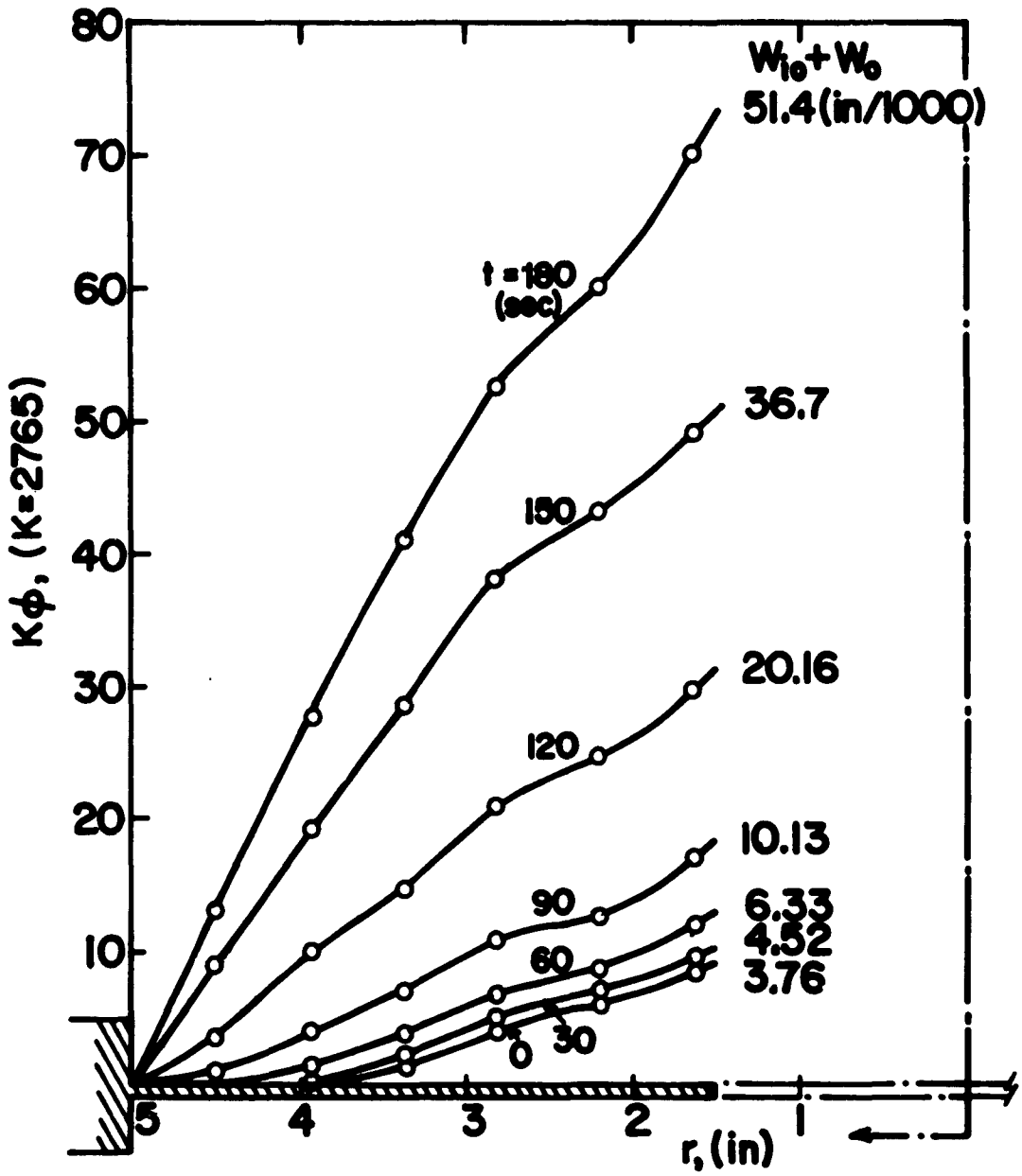

Fig.29. Test No.1 - Change in Slope Distribution with Time

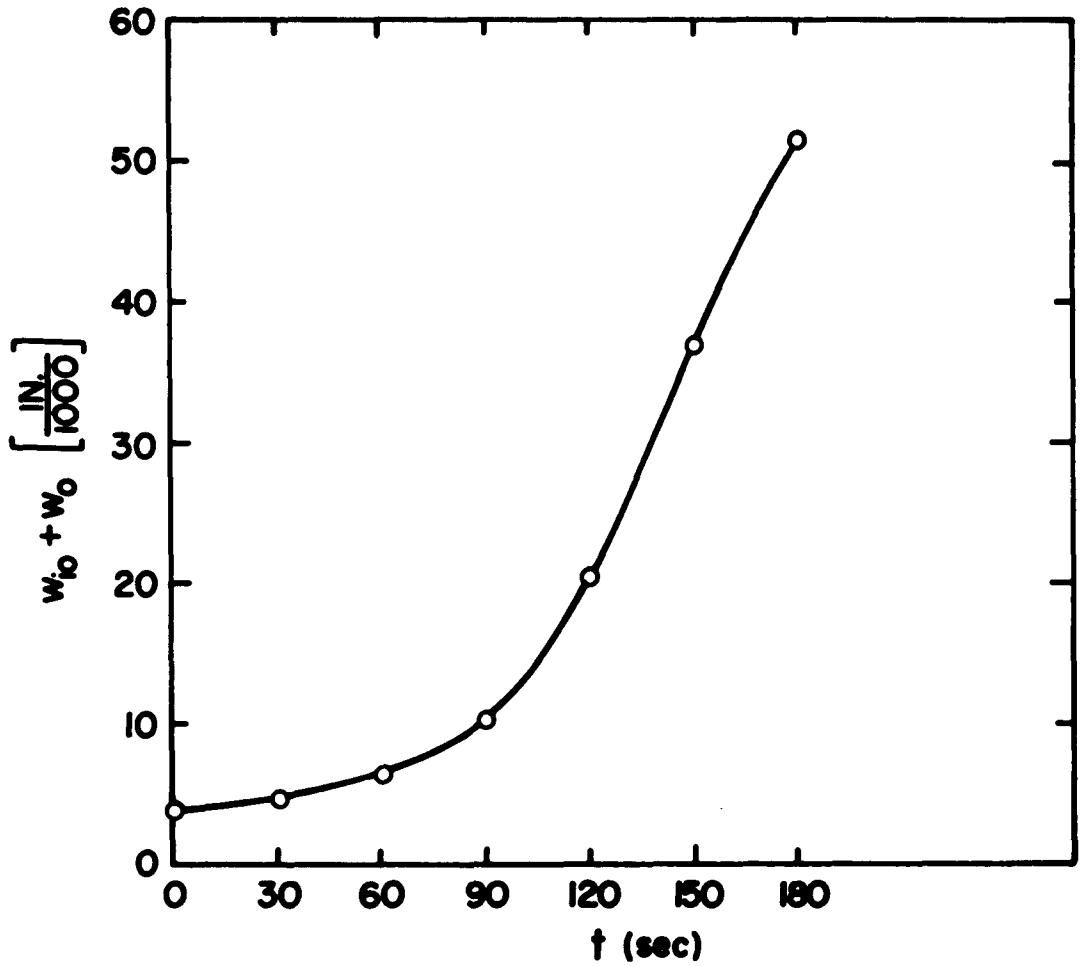

Fig.30. Test No.1 - Total Central Deflection versus Time

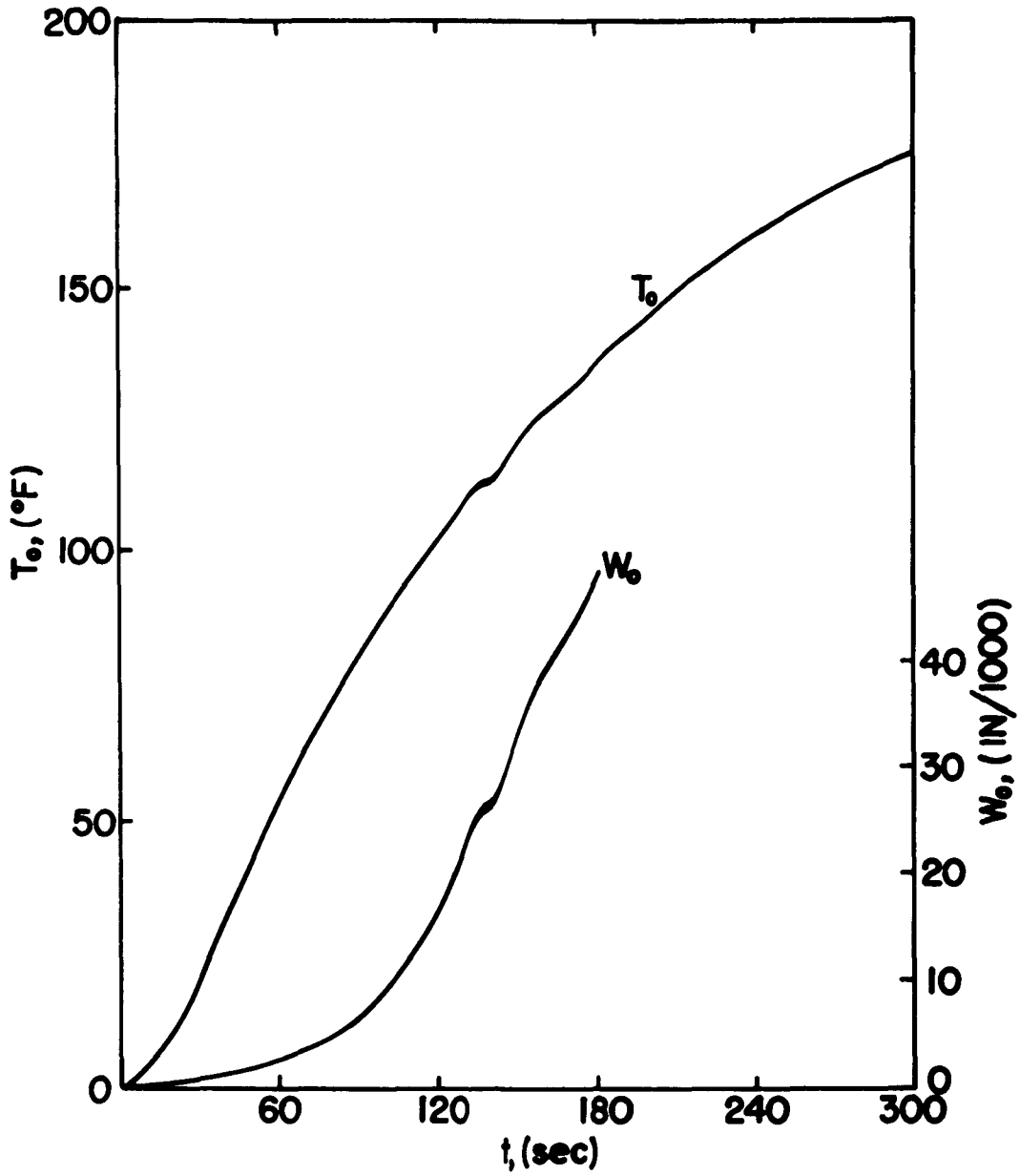

Fig.31. Test No.1 - Central Edge Temperature and Central Edge Deflection versus Time

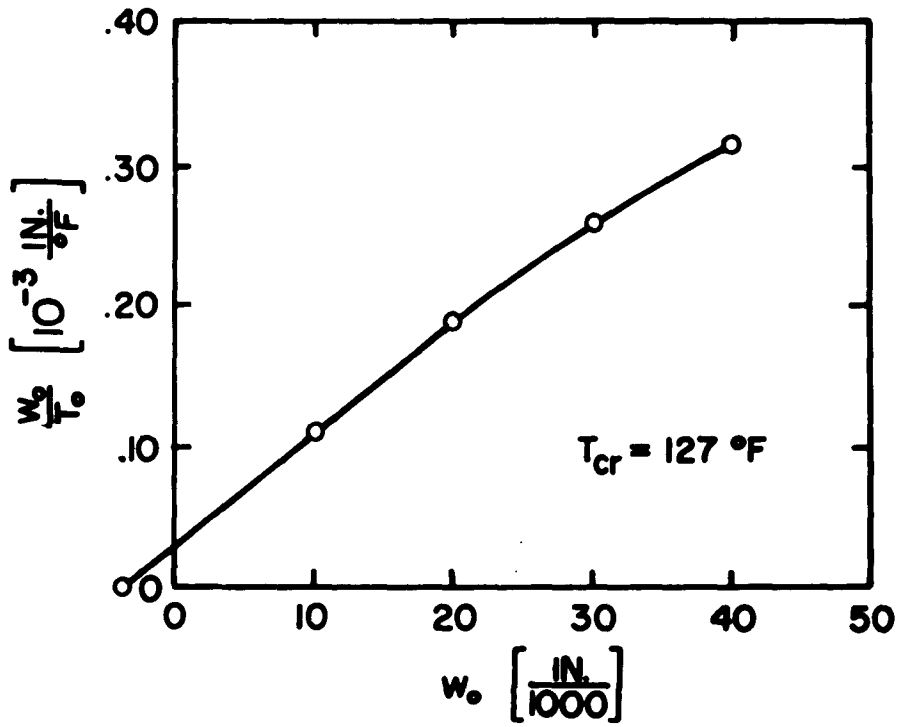

Fig.32. Test No.1 - Southwell Plot

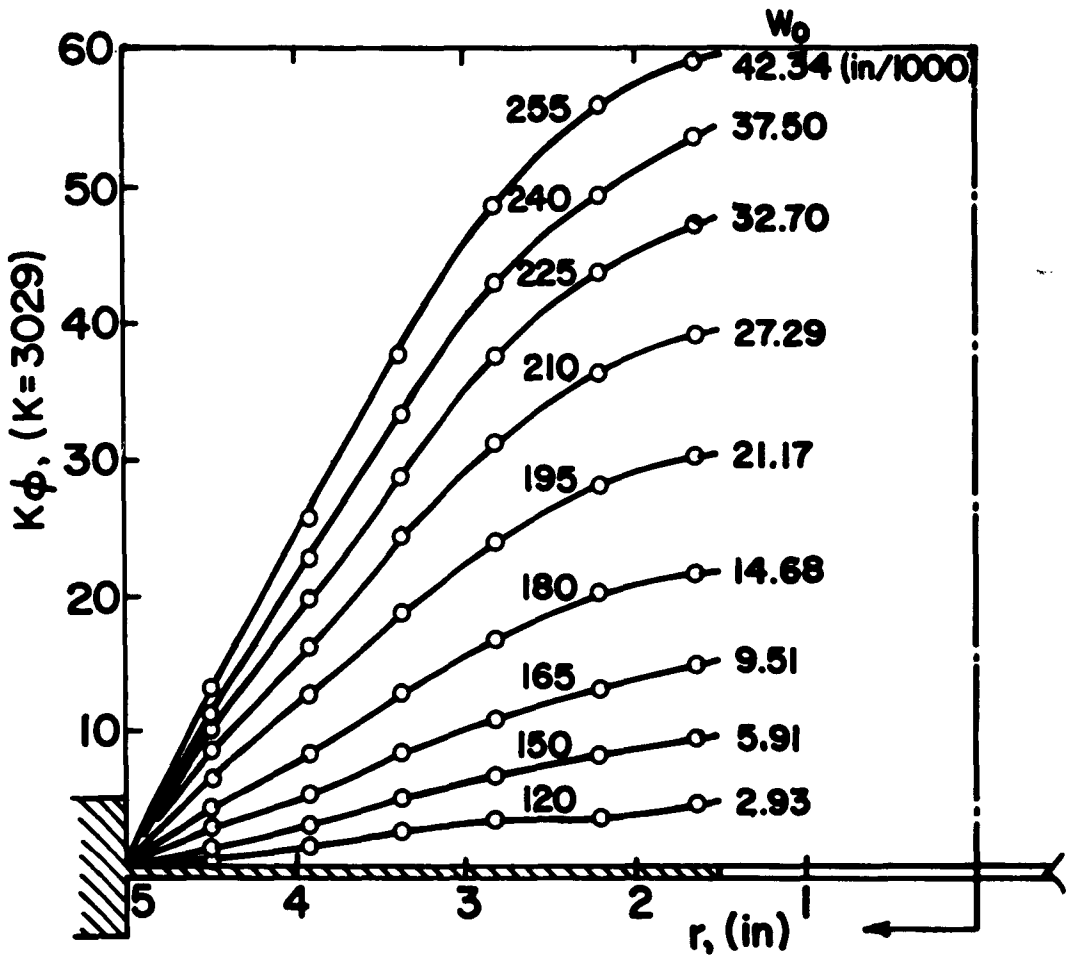

Fig.33. Test No.2 - Change in Slope Distribution with Time

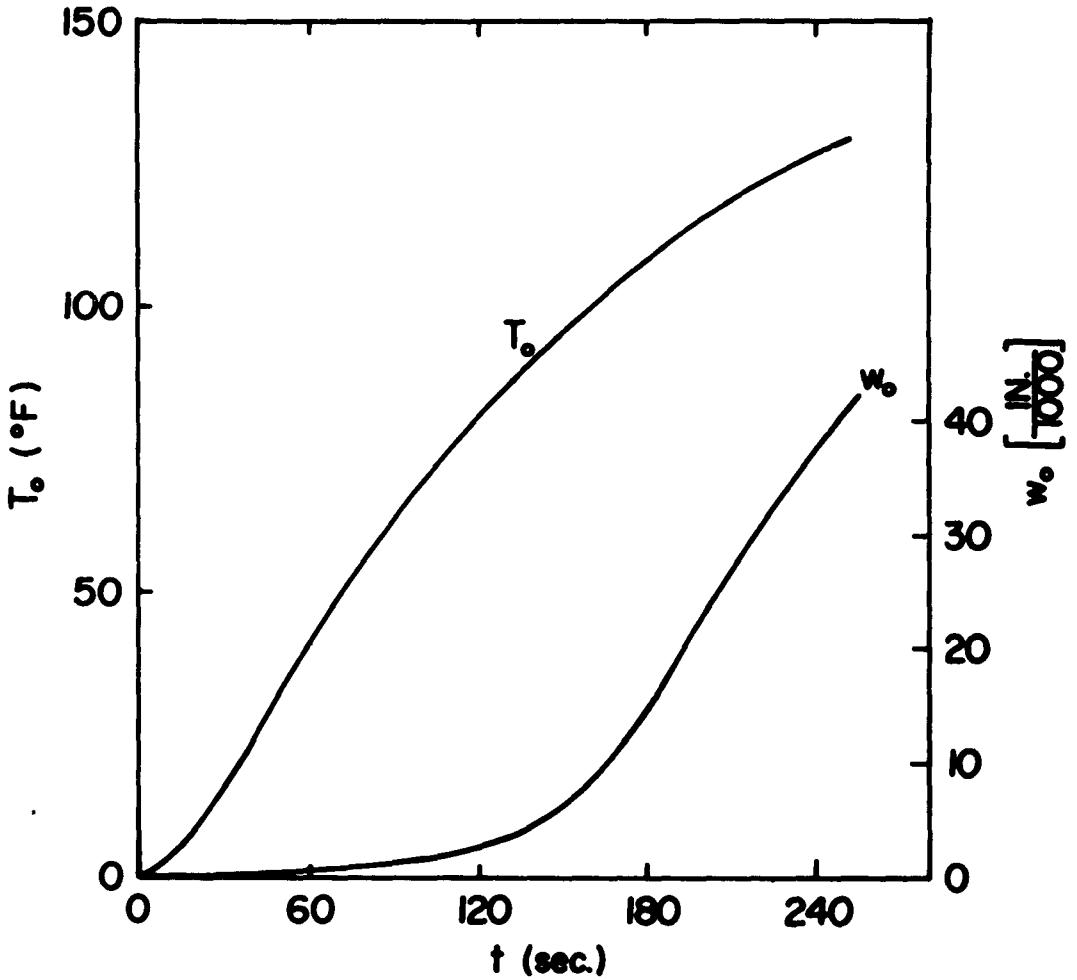

Fig.34. Test No.2 - Central Edge Temperature and Central Edge Deflection versus Time

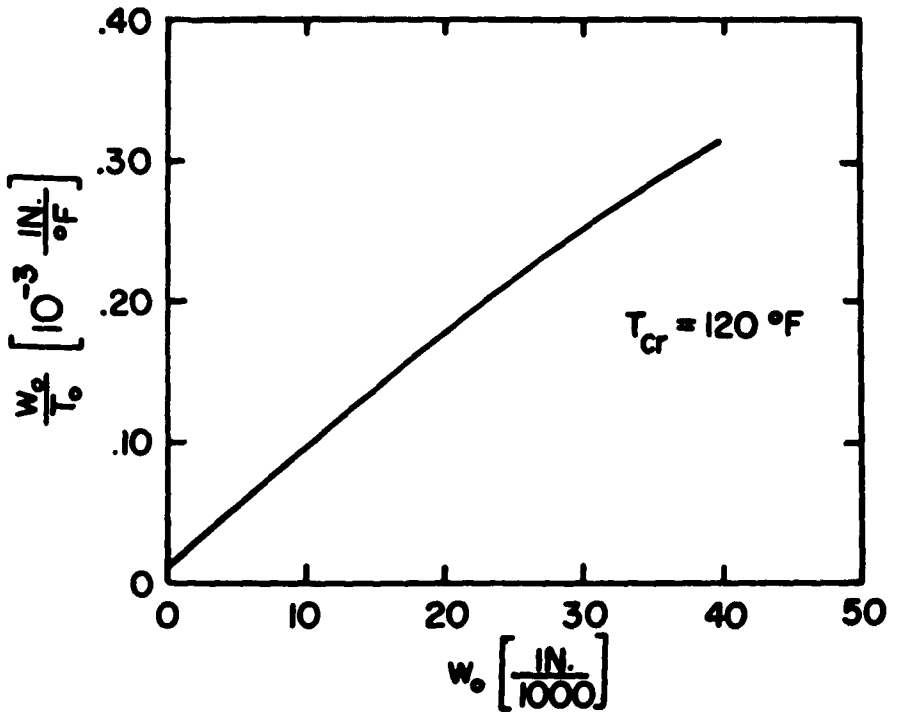

Fig.35. Test No.2 - Southwell Plot

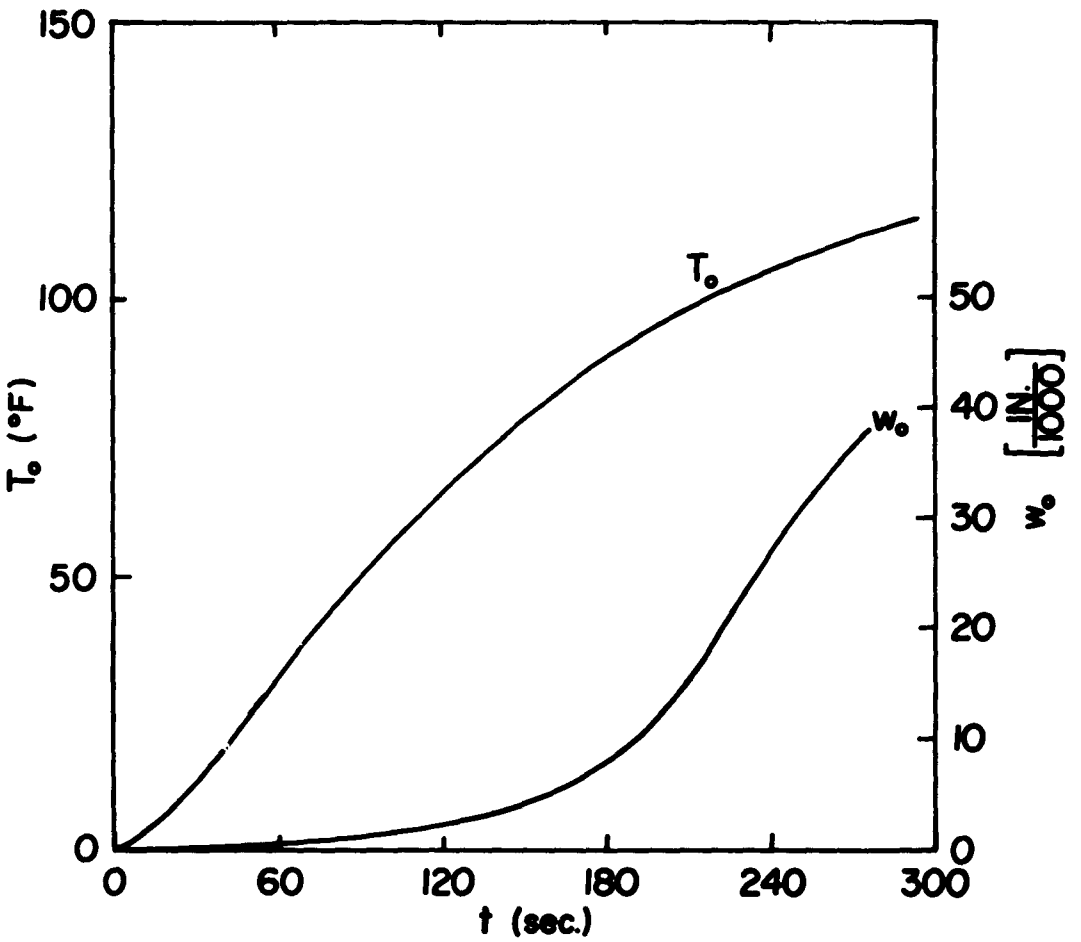

Fig.36. Test No.3 - Central Edge Temperature and Central Edge Deflection versus Time

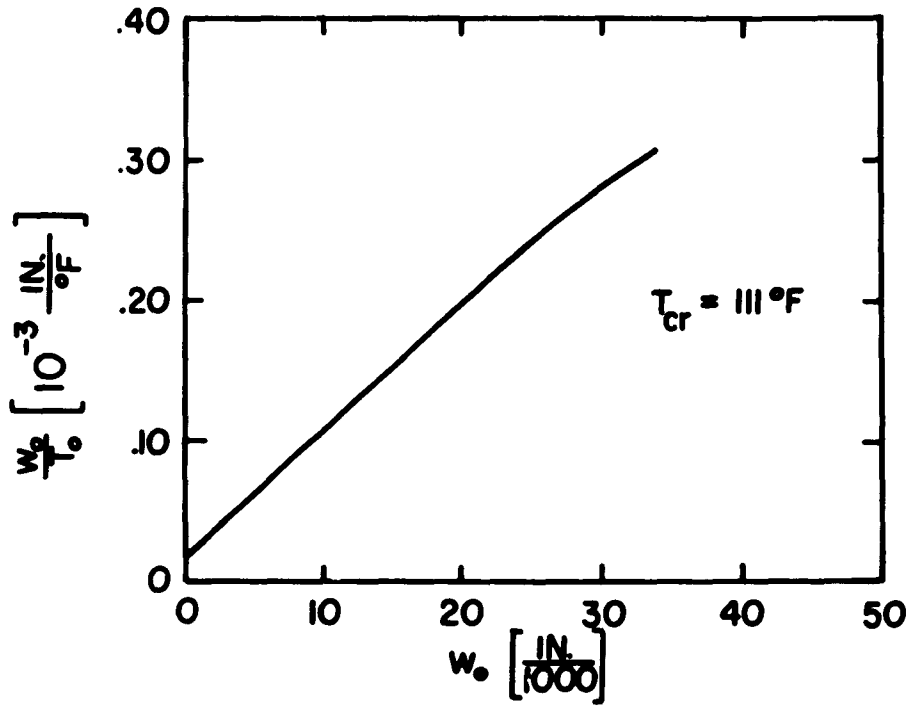

Fig.37. Test No.3 - Southwell Plot

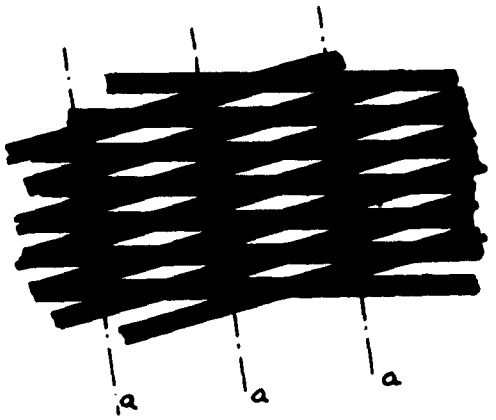

Fig.A-1

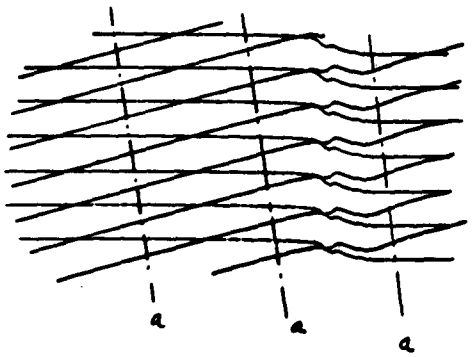

Fig.A-2

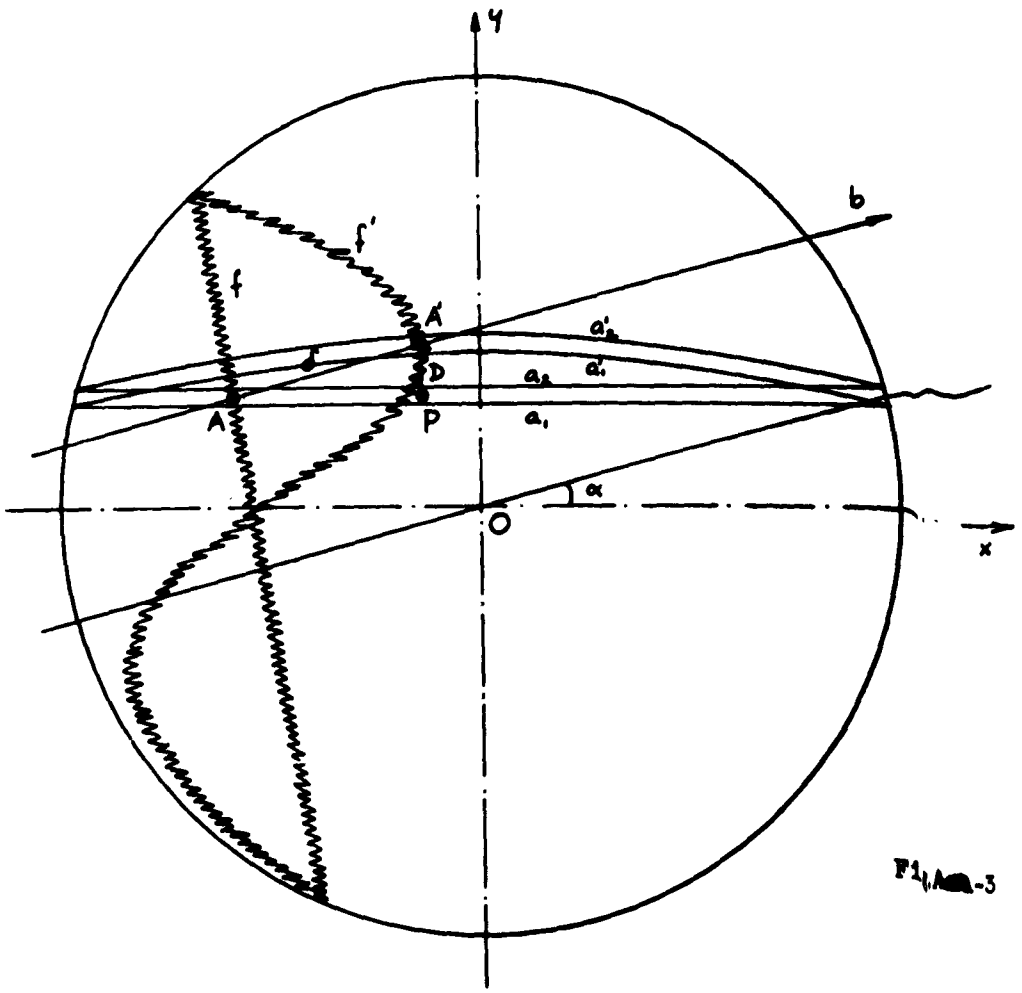

Fig.A-3

Interpretation of Interference Fringes Obtained by the Moire Technique